Palaeogeography, Palaeoclimatology, Palaeoecology 587 (2022) 110798

Contents lists available at ScienceDirect

Palaeogeography, Palaeoclimatology, Palaeoecology

journal homepage: www.elsevier.com/locate/palaeo

Influences on Asian summer monsoon during Dansgaard-Oeschger events 19 to 25 (70–115 kyr B.P.)

Xiao Shi [a,b], Yan Yang [a,b,*], Hai Cheng [c], Jingyao Zhao [c], Ting-Yong Li [d], Lidan Lei [a,b], Sha Liang [a,b], Xiangxiang Feng [a,b], R. Lawrence Edwards [e]

[a] Chongqing Key Laboratory of Karst Environment & School of Geographical Sciences, Southwest University, Chongqing 400715, China
[b] Chongqing Jinfo Mountain Karst Ecosystem National Observation and Research Station, Chongqing 400715, China
[c] Institute of Global Environmental Change, Xi'anJiaotong University, Xi'an 710054, China
[d] Yunnan Key Laboratory of Plateau Geographical Processes & Environmental Changes, College of Tourism and Geography, Yunnan Normal University, Kunming 650050, China
[e] Department of Earth and Environmental Sciences, University of Minnesota, Minneapolis, MN 55455, USA

ARTICLE INFO

Editor: Paul Hesse

Keywords:
Speleothem
Trace element ratios
ASM
MIS 5
92 kyr event
Weak D-O 25

ABSTRACT

The climate variability during Dansgaard-Oeschger (D-O) events 19 to 25 (first recognized in the Greenland ice cores) was recorded in the Asian monsoon region, but the climatological dynamic mechanism is still poorly understood. Here, we present a new ^{230}Th absolute chronology and high-resolution record of the Asian summer monsoon (ASM) from 117 to 69 kyr B.P. based on 25 ^{230}Th ages, 803 oxygen and carbon isotopes, as well as 493 trace element ratios of the YYZ1 stalagmite from Yangzi Cave in Fengdu County, 120 km from Chongqing City, China. The δ^{18}O record supports a strong ASM during marine isotope stages (MIS) 5a and 5c and a weak ASM during MIS 4, 5b, and 5d. Millennial-scale oscillations of D-O 19–25 were also recorded in our speleothem δ^{18}O. Multiple environmental proxies, δ^{13}C and trace element records of YYZ1 stalagmite can also reflect local climate and environmental changes. A drought event was clearly identified between 93.0 and 91.5 kyr B.P., referred to as the 92 kyr event, which exhibited a rapid and abrupt fluctuation (V-shaped) based on our multi-proxy results. We found that D-O 25 event was not obvious in our record and in other Chinese speleothem records. The D-O 25 event occurred within a period of decreasing North Hemisphere summer insolation (NHSI), which led to different climate backgrounds, e.g., the increase of ice volume and the corresponding weakening of the Northern Atlantic thermohaline circulation. Conversely, the D-O events within the high NHSI period or the warm stages (MIS5a, MIS5c) exhibited more obvious fluctuations than those in the low NHSI period or the cool stages (MIS5b, MIS5d). Thus, we suggest that the differences between D-O events are mainly related to the change of the ASM in response to variable NHSI. Furthermore, the ASM during D-O events was also influenced by climate variations in the Southern Hemisphere (SH) and low latitudes, which should not be ignored.

1. Introduction

During the period of marine isotope stage 5 (MIS 5), in the case of relatively low ice volume, the global CO_2 concentration was relatively high, and the seasonal variation in the solar radiation was large (Shackleton, 1987; Petit et al., 1999; North Greenland Ice Core Project Members, 2004; Lüthi et al., 2008). Many speleothem records reveal the close relationship between the Asian summer monsoon (ASM) and the Northern Hemisphere (NH) high latitude climate during this period (Yuan et al., 2004; Kelly et al., 2006; Johnson et al., 2006b; Cheng et al., 2006; Wang et al., 2008; Cheng et al., 2009; Cai et al., 2010; Cheng et al., 2016a). In addition, the changes in the ASM were also influenced by the climate variations in the Southern Hemisphere (SH) (An et al., 2011; Jiang et al., 2016; Zhang et al., 2017; Cheng et al., 2020).

Greenland ice core records indicate that millennial-scale abrupt warming events such as Greenland Interstadials (GIS) 25 to 21 had a significantly long duration and sub-orbital characteristics, which manifested as precursor-type events and rebound-type events (Capron et al., 2010). Moreover, Dansgaard-Oeschger (D-O) (Dansgaard et al., 1993) and Heinrich events (Heinrich, 1988) are the primary climate signals in

* Corresponding author at: Chongqing Key Laboratory of Karst Environment & School of Geographical Sciences, Southwest University, Chongqing 400715, China.
E-mail addresses: sx0919@email.swu.edu.cn (X. Shi), yy2954@swu.edu.cn (Y. Yang), cheng021@umn.edu (H. Cheng), zjyunicorn@stu.xjtu.edu.cn (J. Zhao), fx1996@email.swu.edu.cn (X. Feng), edwar001@umn.edu (R.L. Edwards).

https://doi.org/10.1016/j.palaeo.2021.110798
Received 6 April 2021; Received in revised form 6 December 2021; Accepted 14 December 2021
Available online 18 December 2021

the NH climate archives. Due to contrasting distributions of the external influences on the stadial and interstadial durations, different external climate factors and mechanisms controlled the warming and cooling transitions (Lohmann and Ditlevsen, 2019). Higher-resolution precisely dated speleothem records are needed to constrain the structures and timings of these events and further improve our understanding of their mechanisms. D-O cycles have various features based on visual inspections of several different speleothem records. D-O 25, which exhibits different characteristics than classical D-O events (Oppo et al., 2006), is interpreted as the rebound event at the end of MIS 5.5 (Capron et al., 2010). The speleothem records from low-latitude monsoon regions are relatively few and are inconsistent with those from mid-high latitudes (Drysdale et al., 2007; Boch et al., 2011; Rossi et al., 2014; Dong et al., 2016). In the ASM area, the MIS 5 samples dated within the MIS 5e time range grew slowly(Cheng et al., 2006) and the amplitudes of D-O 25 events' oscillations are weak(Wang et al., 2008; Jiang et al., 2016) due to the low ice volume in the NH and the fact that the millennial-scale changes in the temperature in the North Atlantic region exerted weak effects on the ASM (Zhou et al., 2008). Capron et al. (2012) used the D-O 25 event, which does not have a clear global fingerprint and is inconsistent in the northern high- and low-latitude records, as the basis to determine whether the D-O 25 event was an abrupt global climate event. Additionally, some studies suggested that there was a teleconnection relationship between the East Asian summer monsoon (EASM) and the North Atlantic climate in the early stage of the last glacial period. This coupling relationship is attributed to the periodic changes in the Atlantic thermohaline circulation (Dong et al., 2016). However, missing or indistinct records of the D-O 25 event in the East Asian monsoon region are still in doubt. A detailed record is needed to gain a better understanding of the timing and structure of D-O 25 event.

The interpretation of climate change using speleothem oxygen isotope records is controversial (Ruan et al., 2019; Liu et al., 2020). Climate parameters, such as the temperature and amount of precipitation, are difficult to quantify using only speleothem $\delta^{18}O$ data (Cheng et al., 2019). It is necessary to use new proxies, such as $\delta^{13}C$ and trace elements, to further describe the palaeoclimate variability. Unlike the large regional scale represented by the speleothem $\delta^{18}O$ records, $\delta^{13}C$ records and trace element ratios are indictors of local environmental changes(Fairchild et al., 2000, 2001; Johnson et al., 2006a; Fairchild and Treble, 2009; Zhou et al., 2009).Some studies suggested that these indicators can reflect changes in regional temperature (Zhou et al., 2011), local precipitation (Duan et al., 2016; Zhang et al., 2018), and the productivity and extent of the vegetation cover (Hellstrom and Mcculloch, 2000) in specific areas, which are consistent with or opposite to the explanation of the oxygen isotopes (Cruz et al., 2007; Cheng et al., 2016b). The records from Dongge Cave suggest that the change of trace elements is similar to the $\delta^{13}C$ record for the interglacial epoch (Qin et al., 2004). Moreover, Sr/Ca in speleothem can be regarded as the signals to indicate the variability of the palaeomonsoon, which is affected by atmospheric dust activity and the Asian winter monsoon (Li et al., 2005; Zhou et al., 2009). In Chinese cave records, many AM events, especially weak monsoon events, have the complicated climatological dynamic mechanism (Zhang et al., 2017; Cheng et al., 2019). Because the absolute chronology of ice cores has dating uncertainties and due to the controversy regarding $\delta^{18}O$, multi-proxy records should be used to gain a comprehensive understanding of the various aspects of past environments.

Our study area is in Fengdu County of Chongqing City, southwestern China, which is situated in the interaction zone between the Southwest and East Asian monsoons, making this area sensitive to the monsoon climate. The stalagmite $\delta^{18}O$ records from Yangkou Cave were used to infer the variations in the summer monsoon precipitation and the evolution of the ASM, which was predominantly controlled by the NH solar insolation on orbital timescales (Li et al., 2014). Wu et al. (2020) recently reported the changes in the ASM and regional hydrological conditions during 3.6–118.1 kyr B.P. based on coupled $\delta^{18}O$ and $\delta^{13}C$ records. However, their study lacks higher-resolution, precisely dated speleothem records and trace elements during MIS 5. Therefore, we conducted a multi-proxy study of new and detailed records from Yangzi Cave, which cover MIS 5a–5d, in order to provide insights into the regional nature of the D-O signals and to further elucidate the regional response to climatic conditions and the potential forcing mechanisms.

2. Materials and methodology

2.1. Regional settings

StalagmiteYYZ1 was collected from Yangzi Cave in Fengdu County of Chongqing City, southwestern China (29°47′00″N,107°47′00″E, elevation 330 m) (Fig. 1). The study area is located on the eastern edge of the Sichuan Basin in southwestern China. Multiple parallel-fold mountain systems run through the area, sloping from southeast to northwest, with an average elevation of approximately 750 m. The cave is predominantly composed of the limestone of the Lower Triassic Jialingjiang Formation (Zhu et al., 2004).The study area has a subtropical humid monsoon climate, experiences cloudy and foggy weather, and receives a small amount of light. The climate is mild and the precipitation is abundant throughout the year. Mean annual temperature is approximately constant at 18.3 °C.The average annual rainfall is 1400 mm, and the precipitation in the summer half of the year accounts for nearly three-quarters of the total annual precipitation (Zhang and Li, 2019). The river supplement is dominated by atmospheric precipitation, and most floods occur during summer and autumn. Moreover, the water level in the area exhibits considerable variation.

2.2. Materials and methods

StalagmiteYYZ1, which was used in this study, is narrow on top and at the bottom and wide in the middle, with an oblique cylindrical shape. The sampling length is approximately 950 mm. The stalagmite was cut along its growth axis. The inside of the stalagmite is white, and it is composed of pure and dense calcite without evident impurities, growth striations, and discontinuities in sedimentation. The stalagmite was cut, polished, and washed with ethyl alcohol and deionised water. We used a 1-mm diameter dental drill to obtain 25 ^{230}Th dating samples, and a 0.5-mm diameter drill bit was used to collect samples for the $\delta^{18}O$, $\delta^{13}C$, and trace element analyses at equal intervals along the centre axis of the stalagmite (1 mg for each sample powder). One sample was collected every 0.5-mm in the 0–280 mm region and one sample was collected every 1 mm in the 281–950 mm region to obtain a total of 803 samples. The ^{230}Th ages were determined using a Neptune multi-collector inductively coupled plasma mass spectrometer. All of the results are reported relative to the Vienna Pee Dee Belemnite (VPDB) standard. The analytical details and standard use were described by Cheng et al. (2000, 2013), whilst the chemical experimental procedures followed those described by Shen et al. (2002).

The samples were measured at the Department of Earth Sciences of the University of Minnesota and the Institute of Global Environmental Change of Xi'an Jiaotong University. The samples for the $\delta^{18}O$, $\delta^{13}C$, and trace element analyses were analysed at the Chongqing Key Laboratory of Karst Environments. The oxygen and carbon isotope samples were primarily analysed using a Delta V Plus gas isotope ratio mass spectrometer and a front-end carbonate equipment Kiel-IV. The isotopic data are reported with respect to the VPDB standard with a one-sigma external error of $<\pm0.1‰$ for $\delta^{18}O$ and $< \pm0.06‰$ for $\delta^{13}C$. The results for the parallel samples collected from the stalagmite were $< 0.2‰$.

Approximately 300 μg of $CaCO_3$ samples were dissolved in a 15 mL centrifuge tube using 3% HNO_3. The Ca^{2+} and Mg^{2+} concentrations were measured using the Optima 2100DV inductively coupled plasma (ICP) emission spectrometer (Perkin-Elmer, USA) at the Chongqing Key Laboratory of Karst Environments. The detection limit was 1 μgL^{-1}, and the analytical error was $\leq 2‰$. The Sr^{2+} and Ba^{2+} concentrations were

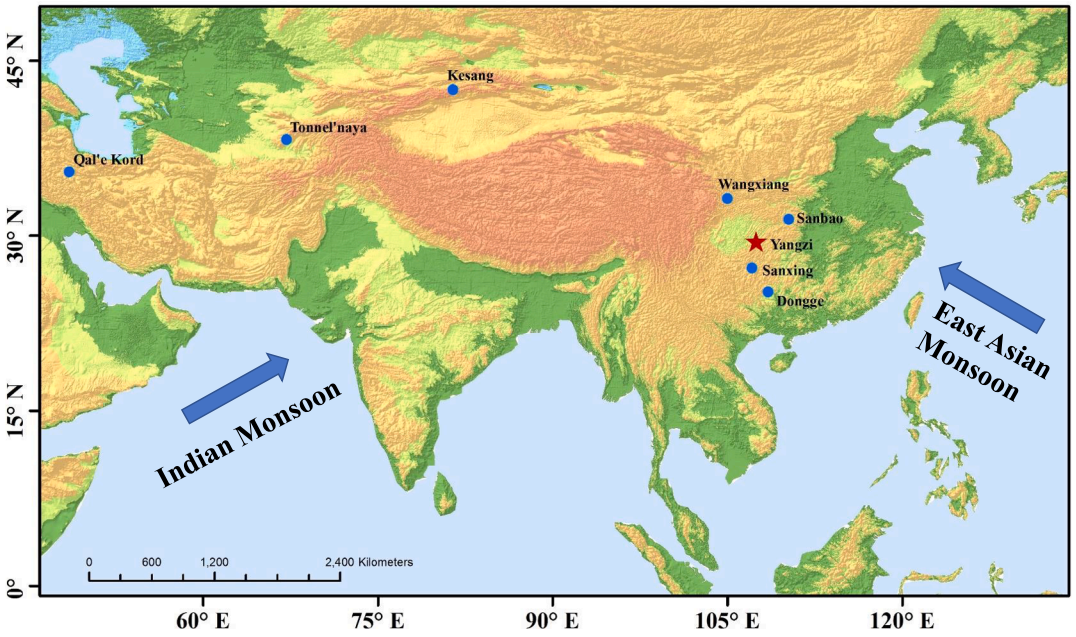

Fig. 1. Location of our study site, Yangzi cave marked with red star.Other cave sites for comparison are marked with blue circles: Wanxiang Cave (Johnson et al., 2006b), Sanbao Cave (Wang et al., 2008), Sanxing Cave (Jiang et al., 2016), Dongge Cave(Kelly et al., 2006), Kesang Cave and Tonnel'naya Cave (Cheng et al., 2016b), Qal'eKord Cave (Mehterian et al., 2017), Blue arrows denote the directions of the East Asian monsoon and Indian monsoon, which affect the climate in China. (For interpretation of the references to colour in this figure legend, the reader is referred to the web version of this article.)

measured using a single-collector ICP mass spectrometry (Element XR, USA) in the same experimental area. The results had a detection limit of 10 ngL^{-1}, and an analytical error of ≤2‰.

3. Results

3.1. Chronology

The sedimentation and dating information for stalagmite YYZ1 are illustrated in Table 1 and Fig. 2, respectively. The ^{238}U contents ranged from 104 ppb to 255 ppb, with an average of 192 ppb. In addition, the ^{232}Th contents ranged from 51 ppb to 5457 ppb, with an average of 569 ppb. The maximum and minimum age errors were ± 553 and ± 164 a, respectively, with a mean uncertainty of ±314 a. The chronological data progressed according to the normal sedimentary characteristics of the speleothem from old to new without age reversal. The growth period of stalagmite YYZ1 was 69–117 kyr B.P., the deposition rate was 0.0047–0.1800 mm/a, the average deposition rate was 0.043 mm/a, and the deposition rate varied significantly. Consequently, the 25 ^{230}Th dates were used to constrain the age-depth relationship of speleothem YYZ1 (Fig. 2) produced using the Constructing Proxy-Record from Age (COPRA) model (Breitenbach et al., 2012). The COPRA model assigned an accurate time scale to the dates using 2000 Monte Carlo simulations and linear interpolation. This model can also be used for repeated and reliable age reversal definitions, error estimations, and hiatus checks.

3.2. $\delta^{18}O$ and $\delta^{13}C$ records

A total of 803 oxygen and carbon isotope samples were analysed and used to reconstruct the δ^{18}O and δ^{13}C curves for 69–117 kyr B.P. period, with an average resolution of 59 a.

The δ^{18}O time series of speleothem YYZ1 varied from −5.47‰ to −9.86‰, with an amplitude of 4.39‰ and an average of −7.84‰. With reference to the Marine Isotope Stages for this timeframe, the period of stalagmite YYZ1 included five stages. During the 116.5–108.3 kyr B.P. period, the δ^{18}O rapidly deviated from −7.09‰ to −5.69‰, and then, it deviated further to −8.21‰. The average δ^{18}O value was −6.68‰. The overall curve showed valley characteristics that correspond to MIS 5d (Fig. 3). During the 108.3–100.7 kyr B.P. period, the δ^{18}O rapidly changed from −8.21‰ to −9.85‰, and became positive by frequent fluctuations, with an average δ^{18}O value of −8.75‰. The overall curve exhibited a peak, corresponding to MIS 5c. During 100.7–83.0 kyr B.P., δ^{18}O rapidly deviated from −8.45‰ to −6.44‰. The average δ^{18}O value was −8.11‰, and it exhibited valley characteristics, corresponding to MIS 5b. Around 83.0–73.7 kyr B.P., the δ^{18}O rapidly changed from −8.28‰ to −9.71‰, with an average δ^{18}O value of −9.06‰, creating a peak, corresponding to MIS 5a. After 73.7 kyr B.P., the δ^{18}O rapidly increased from −8.70‰ to −7.50‰, with an average of −7.94‰. This change represented the beginning of MIS 4.

The δ^{13}C values of stalagmite YYZ1 ranged from −6.70‰ to −12.47‰, with a fluctuation range of 5.76‰ and an average value of −10.62‰. The δ^{13}C of the speleothem was negative during MIS 5b and MIS 5d and positive during MIS 5a and MIS 5c. The average δ^{13}C values during MIS 5d, MIS 5c, MIS 5b, MIS 5a, and the late stage of MIS 4 were − 9.91‰, 11.25‰, 10.69‰, 11.14‰, and 10.53‰, respectively (Fig. 6).

3.3. Trace elements

The trace elements of a total of 493 samples from YYZ1 stalagmite were analysed. The minimum, maximum, and average values of the Mg/Ca ratio were 17.72 × 10^{-3}, 30.80 × 10^{-3}, and 11.36 × 10^{-3}, respectively, whereas those of the Sr/Ca ratio were 0.90 × 10^{-3}, 4.23 × 10^{-3}, and 2.07 × 10^{-3} and those of the Ba/Ca ratios were 1.16 × 10^{-3}, 5.13 × 10^{-3}, and 2.52 × 10^{-3}, respectively. The Mg/Ca, Sr/Ca, and Ba/Ca ratios of stalagmite YYZ1 were relatively similar, and they were all high during the glacial periods (i.e., MIS 5d, MIS 5b, and MIS 4) and low during the interglacial periods (i.e., MIS 5c and MIS 5a). This finding reflected the transition between the glacial and interglacial periods from 117 kyr B.P. to 69 kyr B.P. (Fig. 6).

Table 1
^{230}Th dating results of stalagmite YYZ1.

Sample ID	Depth (mm)	^{238}U (ppb)	^{232}Th (ppt)	[^{230}Th/^{232}Th]	δ^{234}U	[^{230}Th/^{238}U] (activity)	^{230}Th Age (yr BP)
YYZ1-B1	10	174.0 ± 0.2	163.5 ± 3.5	46,296 ± 1000	4217.2 ± 4.4	2.6386 ± 0.0040	69,231 ± 177
YYZ1-B2	30	249.9 ± 0.2	159.0 ± 3.5	68,582 ± 1515	4189.5 ± 4.3	2.6476 ± 0.0043	70,017 ± 164
YYZ1-B4	80	255.4 ± 0.3	131.4 ± 3.1	85,850 ± 2013	4159.5 ± 4.5	2.6785 ± 0.0055	71,616 ± 208
YYZ1-LTY3	100	215.4 ± 0.3	99.9 ± 2.9	95,480 ± 2747	4154.3 ± 9.9	2.6813 ± 0.0045	71,895 ± 240
YYZ1-B6	125	193.8 ± 0.2	89.2 ± 2.5	97,037 ± 2685	4126.8 ± 4.0	2.7106 ± 0.0046	73,343 ± 177
YYZ1-LTY4	175	244.7 ± 0.5	118.2 ± 3.9	93,005 ± 3034	4119.2 ± 14.3	2.7213 ± 0.0063	73,952 ± 353
YYZ1-B8	190	223.1 ± 0.2	437.6 ± 9.3	22,970 ± 492	4096.6 ± 4.7	2.7329 ± 0.0062	74,707 ± 238
YYZ1-B9	240	128.9 ± 0.1	433.2 ± 9.0	13,437 ± 279	4012.2 ± 3.8	2.7396 ± 0.0048	76,631 ± 193
YYZ1-B10	280	104.4 ± 0.1	787.7 ± 15.9	6297 ± 128	4008.9 ± 4.5	2.8822 ± 0.0063	82,034 ± 262
YYZ1-B11	330	230.7 ± 0.3	180.1 ± 4.2	63,355 ± 1478	3903.6 ± 3.7	2.9993 ± 0.0053	89,238 ± 237
YYZ1-LTY7	363	184.9 ± 0.2	650.2 ± 2.8	14,062 ± 66	3869.6 ± 5.9	2.995 ± 0.0063	90,023 ± 305
YYZ1-B12	370	167.8 ± 0.2	5456.6 ± 109.3	1536 ± 31	3874.2 ± 5.5	3.0299 ± 0.0070	91,119 ± 344
YYZ1-B13	410	191.6 ± 0.2	202.0 ± 6.7	47,683 ± 1577	3857.0 ± 3.9	3.0485 ± 0.0063	92,518 ± 289
YYZ1-B14	430	145.1 ± 0.1	463.5 ± 9.9	15,824 ± 338	3851.3 ± 4.6	3.0653 ± 0.0058	93,383 ± 277
YYZ1-B15	480	196.3 ± 0.2	2067.4 ± 41.5	4923 ± 99	3820.1 ± 4.0	3.1444 ± 0.0056	97,680 ± 277
YYZ1-B16	530	199.9 ± 0.1	335.2 ± 7.4	18,774 ± 418	3750.0 ± 4.3	3.1812 ± 0.0068	101,531 ± 343
YYZ1-B17	560	144.7 ± 0.2	108.1 ± 3.2	71,725 ± 2128	3657.8 ± 5.3	3.249 ± 0.0083	107,854 ± 447
YYZ1-B18	580	230.5 ± 0.2	206.0 ± 4.6	59,808 ± 1335	3627.3 ± 3.4	3.2413 ± 0.0050	108,560 ± 276
YYZ1-LTY11	600	166.9 ± 0.2	51.3 ± 10.8	174,975 ± 36,737	3612.0 ± 7.4	3.2583 ± 0.0095	110,071 ± 553
YYZ1-B20	640	226.4 ± 0.2	629.1 ± 13.3	19,113 ± 407	3552.2 ± 3.9	3.2217 ± 0.0065	110,302 ± 365
YYZ1-B22	710	232.8 ± 0.3	959.6 ± 19.6	12,935 ± 265	3505.4 ± 4.9	3.2342 ± 0.0076	112,731 ± 444
YYZ1-LTY14	797	202.3 ± 0.3	96.1 ± 2.7	114,258 ± 3170	3568.7 ± 7.4	3.2878 ± 0.0072	113,214 ± 472
YYZ1-LTY15	877	228.8 ± 0.2	62.9 ± 3.3	197,713 ± 10,454	3544.0.0 ± 6.3	3.2929 ± 0.0069	114,446 ± 439
YYZ1-B29	910	138.7 ± 0.1	115.2 ± 4.0	65,409 ± 2263	3501.3 ± 5.1	3.2932 ± 0.0074	116,060 ± 448

U decay constants: $\lambda_{238} = 1.55125 \times 10^{-10}$ (Jaffey et al., 1971) and $\lambda_{234} = 2.82206 \times 10^{-6}$ (Cheng et al., 2013). Th decay constant: $\lambda_{230} = 9.1705 \times 10^{-6}$ (Cheng et al., 2013).
Corrected ^{230}Th ages assume the initial ^{230}Th/^{232}Th atomic ratio of $4.4 \pm 2.2 \times 10^{-6}$. Those are the values for a material at secular equilibrium, with the bulk earth ^{232}Th/^{238}U value of 3.8. The errors are arbitrarily assumed to be 50%. B.P. stands for 'Before Present' where the 'Present' is defined as the year 1950 CE.
*δ^{234} U = ([^{234}U/^{238}U)$_{activity}$–1) × 1000.

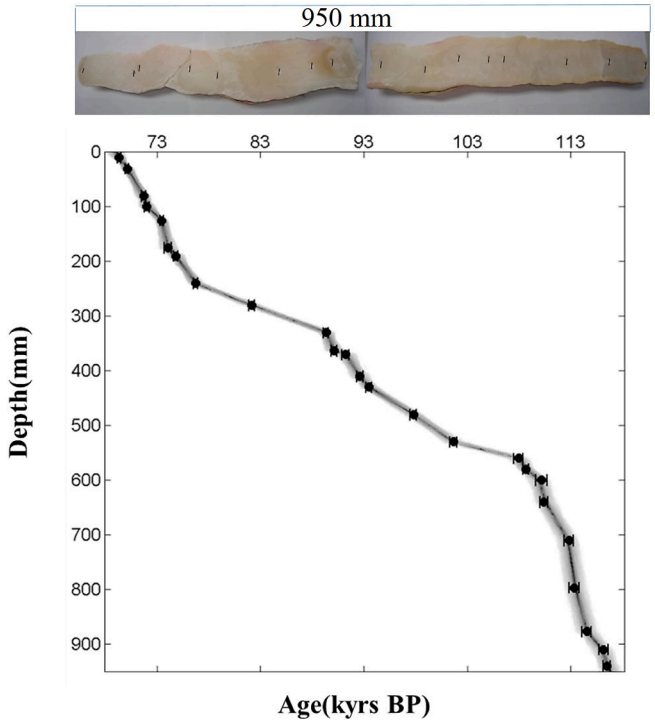

Fig. 2. Age model and photo of YYZ1 stalagmite. Age model is established by COPRA program (Breitenbach et al., 2012),which is based on ^{230}Th dates. Black error bars show ^{230}Th dates with 2σ errors (Table.1).

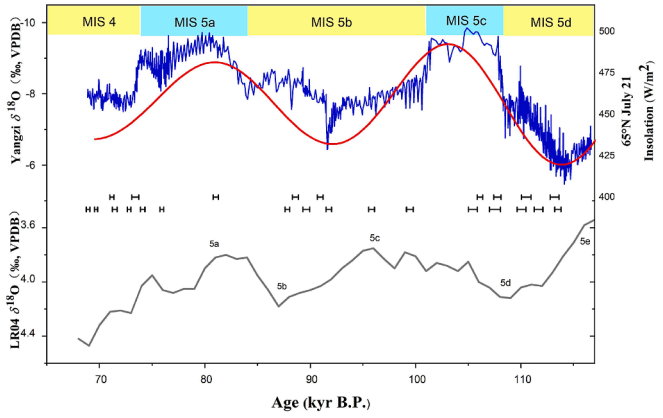

Fig. 3. Comparison of δ^{18}O time series of speleothem YYZ1(blue) with 65°N July Insolation and benthic foraminiferal δ^{18}O-inferred ice volume (gray).^{230}Th ages and errors are colour-coded by speleothem. MIS substagesare listed at the top and bottom. (For interpretation of the references to colour in this figure legend, the reader is referred to the web version of this article.)

4. Discussion

4.1. Reproducibility comparison of the δ^{18}O records of Chinese stalagmites

4.1.1. Timing, duration, and characteristic of the D-O event

Consistent with the changes in the solar radiation records during summer at 65°N, the overall trend of the δ^{18}O variation curve of stalagmite YYZ1 contains three valleys and two peaks similar to the precession fluctuation cycle. That is, the variations in the δ^{18}O record of the stalagmite during this period may have been mainly controlled by the external astronomical orbital parameters on an orbital scale. Compared with the millennial-scale abrupt temperature events (i.e., D-O 19–25 in

the North Greenland Ice Core Project (NGRIP) records), which was conducted using the AICC2012 timescale (Veres et al., 2013), abrupt climatic events were also clearly recorded in the $\delta^{18}O$ record of stalagmite YYZ1. Two of the age control points (108.5 ± 0.2 kyr B.P. and 107.8 ± 0.4 kyr B.P.) were located in the MIS 5d/5c transition stage. The midpoint of this process (108.2 ± 0.3 kyr B.P.) was taken as the onset of MIS 5c. $\delta^{18}O$ was generally negative between 107.8 and 104.6 kyr B.P., with an average value of −9.54‰. At this time, the intensity of the summer monsoon was strong, and this period was defined as D-O event 24. The Sanxing Cave speleothem $\delta^{18}O$ (Fig. 4c) recorded two weak monsoon events during 105.5–104.2 kyr B.P. (with an amplitude of up to 1.5‰). These events were also recorded in Sanbao Cave (Fig. 4b) and Dongge Cave (Fig. 4e) (Kelly et al., 2006) and corresponded to 200–300 years of warm events in the Greenland ice core record. Given the gradual sedimentation and low resolution of the speleothem record from Yangzi Cave during this period, the precursor event (PE) was not evident, but

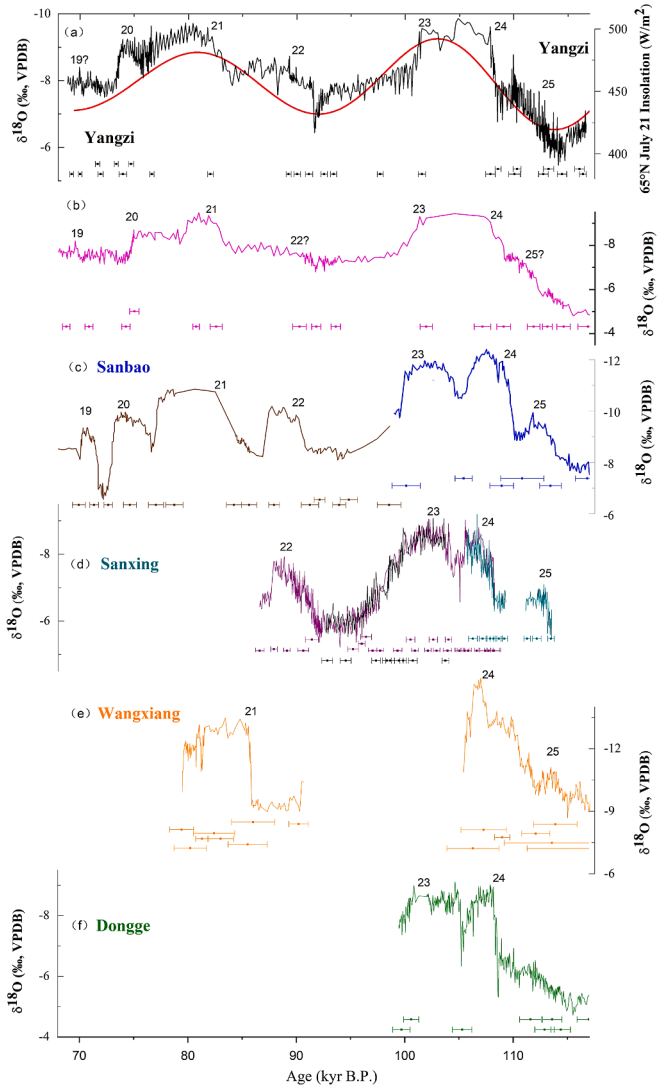

Fig. 4. Comparison of $\delta^{18}O$ records of stalagmite YYZ1 and other records. (a) $\delta^{18}O$ profiles of stalagmiteYYZ1;the red curve shows the 65°N summer Insolation. (b) YZ1 from Yangzi Cave (Wu et al., 2020). (c) SB22,SB23 from Sanbao Cave (Wang et al., 2008). (d) SX7(purple),SX24(black),SX29(dark green) from Sanxing Cave(Jiang et al., 2016). (e) Stalagmite records WX52 from Wanxiang Cave (Johnson et al., 2006b). (f) Stalagmite records D4 from Dongge Cave (Kelly et al., 2006). D-O 19–25 are the millennial-scale warm and humid events in China. (For interpretation of the references to colour in this figure legend, the reader is referred to the web version of this article.)

the trend could be observed continuously during 104.6–103.2 kyr B.P. In the $\delta^{18}O$ record, D-O event 23 started at 103.2 ± 0.3 kyr B.P., which is consistent with the records from Sanxing Cave within the error range. D-O event 22 started at 91.4 ± 0.3 kyr B.P. based on the YYZ1 record, which is comparable to that from Sanxing Cave (91.4 ± 0.6 kyr B.P.) and the SB22 records (90.5 ± 0.8 kyr B.P.). These stalagmite records are basically consistent within the range of the dating error. The timing of the onset of D-O event 21 in the YYZ1 record was inferred to be around 83.9 ± 0.3 kyr B.P. due to a lack of more age-controlling points, which is approximately consistent with the Yangkou (84.6 ± 0.3 kyr B.P.) and Sanbao (83.9 ± 0.7 kyr B.P.) records. The onset and termination of D-O event 20 occurred at 74.7 ± 0.27 kyr B.P. and 73.6 ± 0.3 kyr B.P., respectively, which are identical to the JFYK7 (74.8 ± 0.3 to 73.2 ± 0.3 kyr B.P.; Zhang et al., 2017) and NGRIP records (76.4 ± 2.6 to 74.1 ± 2.6 kyr B.P.) within the error range. The onset of D-O event 19 occurred at 72.3 ± 2.6 kyr B.P. according to the NGRIP record, but in the YYZ1 record, it was indistinct and unresolved. In the same cave, the $\delta^{18}O$ records for stalagmite YZ1 are similar to the YYZ1 record in general, and D-O events 23 and 25 are not obvious (Wu et al., 2020).

The millennium event records of stalagmite YYZ1 include D-O events 22 and 19,possess small amplitudes, and exhibit weak peaks. Moreover, the characteristics of both events are closer to the marine records than to the ice core records. D-O event 19 was distinctly recorded in Sanbao Cave, whereas the amplitude of the variation recorded in Hulu Cave was approximately 1.5 ppm, which is insignificant (Wang et al., 2001). This event was also not apparent in the YYZ1 records, which only exhibited slight variations. Zielinski (2000) believed that the Toba volcanic supereruption event occurred during the transition from MIS 5a to MIS 4, and the Toba volcanic ash was distributed between D-O events 19 and 20. The chronology of D-O events 19 and 20 recorded by stalagmite YYZ1 shows an extremely small deviation from that indicated by the NGRIP records, while D-O event 19 is extremely evident in the NGRIP record. Some studies have suggested that the response of the climate to the Toba volcanic eruptions was not as strong in the low latitudes as in the high latitudes (Wu et al., 2012). This explains why the YYZ1 record gradually declined and fluctuated slightly at 73 ± 0.2 kyr B.P. compared with the NGRIP record, which exhibited a rapid increase and decline. The differences in the initial termination shift between the YYZ1 and NGRIP records were similar to those of the Yangkou Cave and Wanxiang Cave records. Thus, we speculate that the climate change at low latitudes played a crucial role during this period (Du et al., 2019).One possible hypothesis is that the millennial events that occurred during the glacial period were triggered in the high latitudes in the NH (Broecker, 1998), whereas the interglacial events were triggered in the SH (Bakker et al., 2017) or low latitudes (Wang, 2006). This research field is complicated and challenging, but it is crucial to understanding the orbital-millennial climate changes and the relationship between low latitude and global changes (Cheng et al., 2019).

4.1.2. Factors controlling the stalagmite $\delta^{18}O$ records

The benthic δ18O records define 24 new marine isotope stages (MIS) in the early Pliocene, which accounts for a large percentage of the records from the Atlantic and is related to Northern Hemisphere insolation. The uncertainty in the LR04 age model is derived from the sedimentation rate constraints and the assumed response times of the ice sheets. In contrast to this, our speleothem records possess a 20 kyr precession cycle, which represents the change in the East Asian summer monsoon.

In terms of isotope fractionation, the major factors affecting the stalagmite $\delta^{18}O$ values are the cave temperature and drip water (Hendy, 1971). The effect of the cave temperature on the $\delta^{18}O$ fractionation coefficient is −0.23‰/°C (Oneil et al., 1969). Compared with the ~3 °C temperature change obtained from $\delta^{18}O$ simulation results of cave speleothems in southern Asia (Caley et al., 2014), we infer the variation in temperature during the entire depositional period of stalagmite YYZ1 was approximately 19 °C. These two results are significantly different.

Thus, temperature is not the dominant factor affecting the $\delta^{18}O$ changes in the YYZ1 record. Given the combined influence of the Indian summer monsoon (ISM) and the East Asian summer monsoon (EASM), interpreting the stalagmite $\delta^{18}O$ records in this region is relatively complicated. In the monsoon region of China, the stalagmite $\delta^{18}O$ indicates the average summer monsoon intensity (Cheng et al., 2012a). Isotope modelling supports the conclusion that the $\delta^{18}O$ records represent the intensity of the EASM system (Liu et al., 2014). Modern meteorological observation data indicate that the water vapour for the summer precipitation in the EASM region mainly comes from the Indian Ocean (Ding et al., 2004; Drumond et al., 2011). The stalagmite $\delta^{18}O$ record (mainly including MIS 5a, 5c, and 5e) from Tianmen Cave, which is located in the area affected by the ISM, shows that the change in the ISM intensity is basically consistent with that of the EASM, that is, there are no evident phase differences between the ISM and EASM (Cai et al., 2010).Therefore, the enhancement of ISM or EASM on the orbital and millennial scale was regarded as the enhancement of ASM. The record from northern India also suggests that the ISM and ASM exhibit a coupled response to the changes in the NH summer insolation without significant temporal lags (Cheng et al., 2016a). In addition, the $\delta^{18}O$ values indicate the strength of the southerly monsoonal flow over East Asia (Liu et al., 2014).Yangzi Cave is located in the area in which the ISM and EASM interact, which is highly sensitive to the changes in the monsoon climate. The stalagmite $\delta^{18}O$ values reflect the changes in overall entire ASM intensity (Zhang and Li, 2019). Heavier $\delta^{18}O$ values indicate weak summer monsoon intensity, and vice versa.

4.1.3. *Variability of D-O 25 event*

Whether the D-O 25 event was a global climate event remains controversial. The D-O 25 event was a significant sub-orbital abrupt climate event with a long duration in the NGRIP record. The $\delta^{18}O$ record of stalagmite YYZ1 contains an abrupt negative shift at 113.0 ± 0.4 kyr B.P. (amplitude of up to 5%), implicating the onset of the D-O 25 event. This event is consistent with the Sanxing Cave (113.1 ± 0.4 kyr B.P.) (Jiang et al., 2016) and Sanbao Cave (112.3 ± 0.8 kyr B.P.) records (Wang et al., 2008) within the error range. The $\delta^{18}O$ values of the Sanbao Cave record gradually became negative with no sudden abrupt negative shift, reflecting a weak monsoon intensification event. However, we found this quite surprising given that such an event is not visible in all of the Chinese records. The $\delta^{18}O$ trend changes at ~113 kyr B.P., but there is no clear peak in these records. Due to the lower temporal resolution of the $\delta^{18}O$ record, the D-O 25 event is not obvious in the YZ1 record (from the same cave) (Wu et al., 2020). In addition, the D-O 25 event was not clearly recorded in Suozi Cave (Fig. 5g) and Dongge Cave (Fig. 5f). At middle and high latitudes, the L4 speleothem in Dragon Cave distinctly recorded the beginning of the D-O 25 event at 113.9 ± 0.6 kyr B.P. However, the timing of the end of this event is unclear because of the growth discontinuity in the stalagmite, but it is inferred to have ended at 111.3 ± 0.6 kyr B.P. (Dong et al., 2016). Located at the edge of the area affected by the summer monsoon, the onset of the D-O 25 event was recorded in Wanxiang Cave at 114.5 ± 3.4 kyr B.P. However, the large dating error for the end of the record has resulted in the imprecise calibration of the age (Johnson et al., 2006b). Through comparison of the relevant records, the high- and low-latitude stalagmite records in China were determined to exhibit good consistency with the D-O 25 event, indicating that the event is a regional Asian summer monsoon enhancement event. According to the existing speleothem records in the Asian monsoon region, the amplitude of the D-O 25 event is smaller than that of the other climate fluctuation events on the millennial and centennial scales. The D-O 25 event occurred at the low NHSI period. An initial increase in the solar radiation in the NH and a similar event (D-O 22) also occurred during the same type of stage. However, the D-O 22 event is more evident in the speleothem records in the monsoon region than D-O 25 event. Therefore, the amount of solar radiation is not the only reason for the small amplitude of the D-O 25 event in the records. The period of initial ice sheet build up is considered

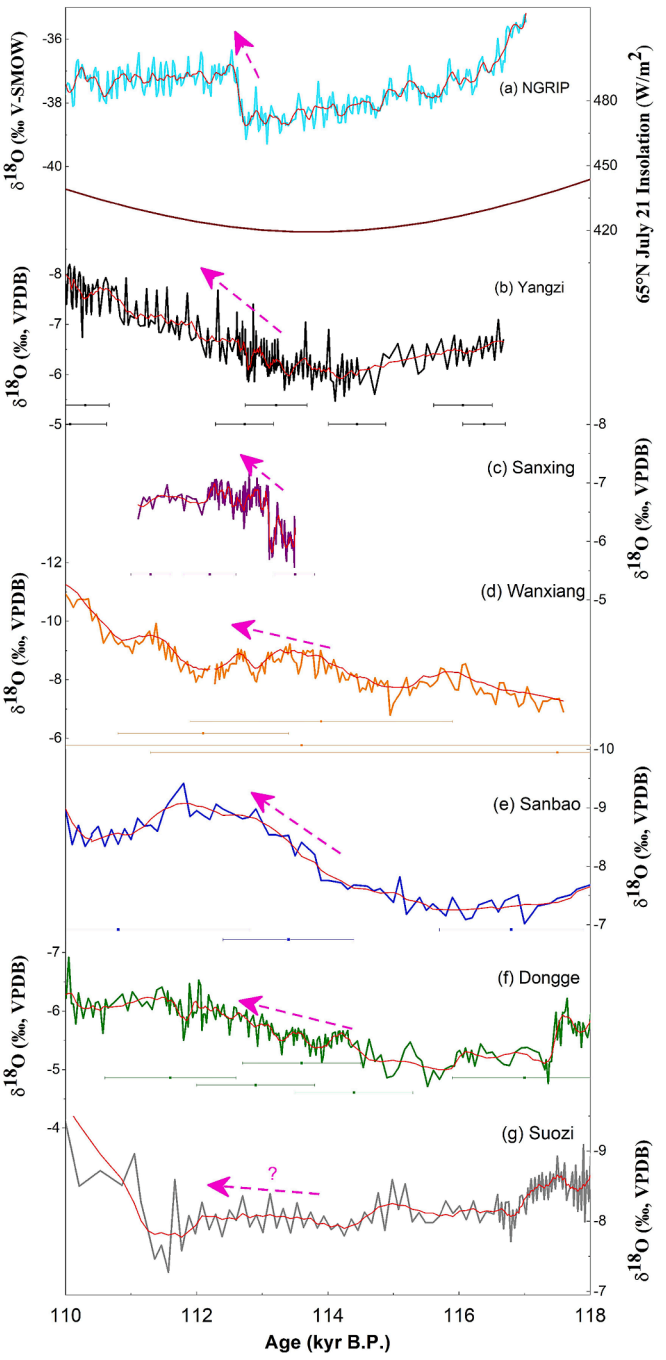

Fig. 5. Detailed comparison between YYZ1 and other records of D-O25 event. (a) NGRIP(AICC2012 time-scale, Veres et al., 2013). (b) $\delta^{18}O$ records of stalagmite YYZ1. (c) SX29 from Sanxing Cave (Jiang et al., 2016). (d) WX52 from Wanxiang Cave (Johnson et al., 2006b) (e) SB23 from Sanbao Cave(Wang et al., 2008). (f) D4 from Dongge Cave (Wang et al., 2008). (g) SZ2 from Suozi Cave (Kelly et al., 2006).The purple curve shows 20 pts. SG smooth of their stalagmite records, respectively. (For interpretation of the references to colour in this figure legend, the reader is referred to the web version of this article.)

the reason for the weak amplitude of the D-O 25 event, but the characteristics of the D-O 25 event are similar to those of other D-O events. In the YYZ1 record, the amplitudes of D-O events 19, 22, and 25 are smaller than those of other D-O events, which is consistent with the Greenland ice core record (Andersen et al., 2004). Thus, the triggering mechanism of this event cannot be simply attributed to the melting of ice or another large freshwater input to the North Atlantic Ocean. The partial or complete shutdown of the Atlantic Meridional Overturning Circulation

(AMOC) is the primary cause of and explanation for the stadial occurrences (Rahmstorf, 2002). During the warm period of MIS 5e, the AMOC experienced three long periods of strong weakening (Galaasen et al., 2014). During MIS 5b and 5d, the sea surface temperatures decreased less in the western tropical Atlantic than in the Atlantic Ocean at high latitudes, suggesting the decoupling of the tropical and northern high-latitude areas during the low intensity AMOC(Rama-Corredor et al., 2015). Beck et al. (2018) argue that neither the EASM intensity nor the Chinese cave $\delta^{18}O$ records are governed by high-northern-latitude insolation, but rather by the low-latitude inter-hemispheric insolation gradients, which may strongly influence the global ice volume via monsoon dynamics. During MIS 5d, which has just passed through the peak period of the last interglacial period, the Thermohaline Current (THC) in the North Atlantic was weak. Consequently, the temperature variation in the North Atlantic region was weakly transmitted to the ASM and was mainly affected by the processes in the low latitudes.

4.2. Coupling of speleothem $\delta^{13}C$ and trace elements

The latest research shows that speleothem $\delta^{13}C$ values can be used as a proxy for climate conditions, and they reflect the changes in the external environment (Fohlmeister et al., 2020). A local modern environmental monitoring study in the Chongqing area also revealed that the evolution of the Asian summer monsoon is recorded by speleothem $\delta^{13}C$ records (Li et al., 2018). The $\delta^{13}C$ and $\delta^{18}O$ records of stalagmite YYZ1 exhibit synchronous changes on the millennial scale (Fig. 6, Table2). During MIS 5a and MIS 5c, the enhancement of the summer monsoon and the higher local precipitation resulted in lower $\delta^{13}C$ values in southwestern China, and vice versa. Speleothem $\delta^{13}C$ values were significantly more positive during periods of lower solar radiation (115–111 kyr B.P., 94–91 kyr B.P., and 72–69 kyr B.P.), which indicates that the changes in the dry and wet conditions in Yangzi cave obviously respond to the ASM and the weakening of the NHSI intensity on the orbital scale. However, no evident negative $\delta^{13}C$ peak similar to the $\delta^{18}O$ peak was observed during the warm MIS 5c and MIS 5a periods or the strong summer monsoon stage. Therefore, other factors should be considered when assessing the indicative significance of the $\delta^{13}C$ record of stalagmite YYZ1. Stalagmite $\delta^{13}C$ values are affected by several

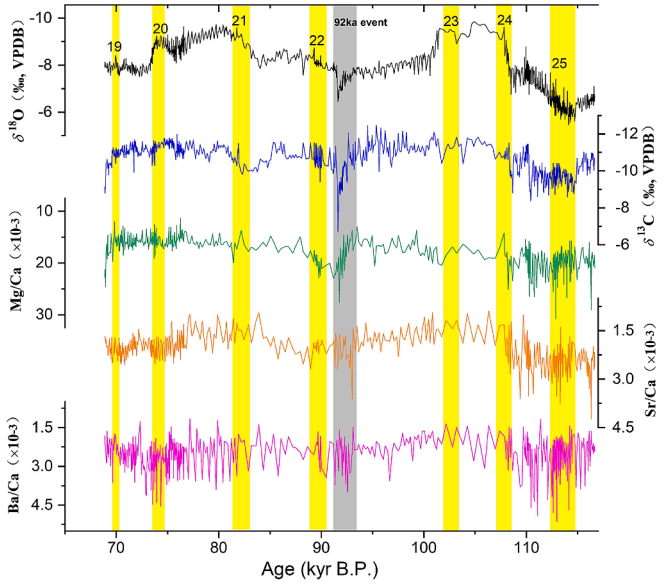

Fig. 6. $\delta^{18}O$, $\delta^{13}C$ records and the trace elements ratios from YYZ1.$\delta^{18}O$ record (black); $\delta^{13}C$ record(blue);Mg/Ca ratio(green);Sr/Ca ratio(orange);Ba/Ca ratio (pink). The gray bar indicates the "92kyr event" of weak ASM. (For interpretation of the references to colour in this figure legend, the reader is referred to the web version of this article.)

factors, such as variations in the regional temperature and humidity, vegetation types and coverage, the karst water transport time, and the prior calcite precipitation (PCP) effect (Dorale et al., 1998; Genty et al., 2003).Chongqing is located in a subtropical region, and C3 plants are the dominant type of vegetation. It is considered that the carbon isotope composition is about −25‰ for overlying C3 plants, but the $\delta^{13}C$ of the associated speleothem ranges from −12‰ to −4‰ (Genty et al., 2003; McDermott, 2004). A previous study on Yangzi Cave also supported this conclusion (Wu et al., 2020).The variation range of the $\delta^{13}C$ of stalagmite YYZ1 was not significant during the warm periods. Do the lower $\delta^{18}O$ values, which reflect an enhanced summer monsoon not necessarily indicate an increase in precipitation? Actually, influenced by too much precipitation, faster karst flow rates, shorter water-soil residence times, and a lack of isotopic-equilibrium between soil CO_2 and water will all result in lower $\delta^{13}C$ speleothem values (Baker et al., 1997; Li et al., 2018). This pattern has been observed in Soreq Cave in Israel (Bar-Matthews et al., 2000) and Clamous Cave in southern France (Plagnes et al., 2002). That is, a strong summer monsoon leads to heavy precipitation (the over wet model), and the rapid flow of soil water in an extremely humid climate shortens the residence time of the soil water. This may prevent the dissolution equilibrium of CO_2 from being reached, and the $\delta^{13}C$ speleothem values will decrease.

The interpretation of $\delta^{13}C$ records is complex and uncertain, even for stalagmites from the same cave (Fohlmeister et al., 2020). Other proxies, especially the Mg/Ca, Sr/Ca, and Ba/Ca ratios, are helpful in more detailed climate reconstructions. The trace element ratios of stalagmite YYZ1 were low during the warm periods and high during the cold periods. The highly resolved trace element reconstruction exhibited millennial-scale variability corresponding to D-O events 19–25 (yellow region in Fig. 6). The comparisons between the trace element ratios and the $\delta^{18}O$ and $\delta^{13}C$ values indicate that Mg/Ca and $\delta^{13}C$ are strongly correlated on the millennial scale. There is a significant positive correlation ($r = 0.325$, $p < 0.01$) between the Mg/Ca and $\delta^{13}C$ values (Table 2). Several case studies have effectively used trace elements (e.g., speleothem Mg) as records of palaeoaridity (Fairchild and Treble, 2009). Extended groundwater residence times and enhanced water-rock interactions (WRIs) are beneficial to increasing the Mg contents of cave deposits. The residence time is closely related to the external dry and wet conditions and the precipitation changes (Verheyden et al., 2000; Treble et al., 2003). Wet conditions lead to enrichments in Mg and Sr compared to Ca, due to the selective leaching of Mg and Sr. Stalagmite YYZ1 is pure calcite, and there is no transformation of aragonite to calcite. We did not consider the influences of temperature, deposition rate, and mineral variations on the partition coefficients, which affect the Mg and Ca contents of the speleothem. The partition coefficients for Mg are always much less than one. The correlation between the Mg/Ca and $\delta^{13}C$ values reflects the PCP effect caused by CO_2 degassing during karst water transport. During the MIS 5c and MIS 5a monsoon enhancement stages, the monsoon precipitation increased, resulting in rapidly flowing karst water and shorter reaction times, which led to a decrease in the Mg/Ca values of stalagmite YYZ1. During the period with less precipitation, the longer residence times and water-rock interaction times strengthened the CO_2 degassing and PCP, resulting in higher Mg/Ca ratios. Cold and dry climates promote atmospheric dust and increase the Sr concentrations of speleothems (Jahn et al., 2001; Li et al., 2005; Zhou et al., 2009). The change in Ca^{2+} with PCP had a significant influence on the change in the Sr/Ca ratio (Johnson et al., 2006a, 2006b; Cruz et al., 2007; Zhang and Li, 2019). The Ba/Ca and Sr/Ca ratios are significantly correlated in stalagmite YYZ1($r = 0.329$, $p < 0.01$), suggesting that they may have been subject to a common control mechanism.

During the periods with the lowest solar radiation at 65°N (i.e., at 115–111 kyr B.P., 94–91 kyr B.P., and 72–69 kyr B.P.), the $\delta^{13}C$, Mg/Ca, Sr/Ca, and Ba/Ca values of stalagmite YYZ1 exhibited extreme changes, with a negative $\delta^{13}C$ excursion and rapidly increasing Mg/Ca, Sr/Ca, and Ba/Ca values. These results showed that during the cold periods, the

Table 2
Correlation coefficients between $\delta^{18}O$, $\delta^{13}C$ and trace element ratios of stalagmite YYZ1.

	O	C	Mg/Ca	Sr/Ca	Ba/Ca
O	1	0.577**	0.179**	0.349**	0.106*
C	–	1	0.325**	0.100*	−0.081
Mg/Ca	–	–	1	0.297**	−0.1*
Sr/Ca	–	–	–	1	0.329**
Ba/Ca	–	–	–	–	1

* Indicates significant at a 95% confidence level ($p < 0.05$).
** Indicates significant at a 99% confidence level ($p < 0.01$).

ASM intensity weakened, the climate became dry, the migration time of the dripping water in the cave was prolonged, and the PCP was enhanced, thereby resulting in changes in the $\delta^{13}C$, Mg/Ca, Sr/Ca, and Ba/Ca values of the speleothems. In contrast, as the solar radiation gradually reached the maximum value, the $\delta^{18}O$ decreased. This suggests that the intensity of the ASM increased, leading to more precipitation. The YYZ1 records show covariations between the Mg/Ca, Sr/Ca, and Ba/Ca ratios, which all decreased significantly. We conclude that the coupling between the changes in the $\delta^{13}C$ values and the trace element ratios reflects the changes in local ecological environment.

4.3. Multiproxy record and mechanism of the 92 kyr weak monsoon event

The $\delta^{18}O$ values of YYZ1 rapidly fluctuated between 93.1 and 91.5 kyr B.P., which rapidly became negative when the highest positive value was reached at 91.6 kyr B.P. The amplitude of this variation is 1.4‰, and it is generally V-shaped. In addition, the duration of the event was approximately 1.5 kyr B.P. We found that the AM records (i.e., the $\delta^{18}O$ records of stalagmites after smoothing out the solar radiation signals) exhibited a downward trend during 91–93 kyr B.P. During this period, the $\delta^{18}O$ values of the Sanxing, Sanbao, Xiaobailong, and QK cave records all reached and maintained their lowest values for a period of time (Jiang et al., 2016; Wang et al., 2008; (Cai et al., 2015); (Mehterian et al., 2017)). However, two hiatuses occurred during periods of unstable climate and one of them interrupted the growth of the stalagmite in other records (Columbu et al., 2019). Small deviations occurred in the times recorded and in the magnitudes of the $\delta^{18}O$ variations in the different caves. The speleothem records from Sanxing Cave gradually became positive after 97.6 kyr B.P., reaching the most positive value from 95.8 kyr B.P. to 92.4 kyr B.P., and they gradually became negative thereafter (Fig. 7b). The $\delta^{18}O$ record from Sanbao Cave reached the maximum at 94.9 kyr B.P. and became negative after 91.3 kyr B.P. (Fig. 7c).This weak monsoon event was also recorded in mid-latitude areas, such as in Kesang Cave in Xinjiang (Cheng et al., 2012b) and in Tonnel'naya Cave in Uzbekistan (Cheng et al., 2016b). The speleothem record of the former rapidly deviated after 94.1 kyr B.P. until it reached the maximum at 93.9 kyr B.P., and then, it rapidly deviated again at 93.9–92.3 kyr B.P. From 93 to 90 kyr B.P., a 0.8‰ enrichment in the oxygen isotopic values led to the highest $\delta^{18}O$ values in the stalagmite K1–2010 record (Nehme et al., 2015). The regional differences in the oxygen isotopes of the speleothem on this short time scale may have been caused by the differences in the hydrothermal patterns caused by the different land/ocean distribution patterns in the East Asian and Indian monsoon regions (Tan et al., 2009). Cheng et al. (2012a) discovered that the influence range of the ASM can extend to the interior part of Central Asia when the solar radiation increases, and atmospheric circulation can replace temperature as the dominant factor controlling the variations in $\delta^{18}O$ in these areas. During the period of low solar radiation in the NH, the $\delta^{18}O$ values in Kesang Cave were positive because the weakening of the summer monsoon exacerbated the evaporation in the local lake basin. This phenomenon caused the local water vapour's $\delta^{18}O$ value to increase and made the directly inherited $\delta^{18}O$ value of the atmospheric precipitation positive. We conclude that the rapid and positive change in the $\delta^{18}O$ value in the stalagmite YYZ1 record at 93.1–91.5

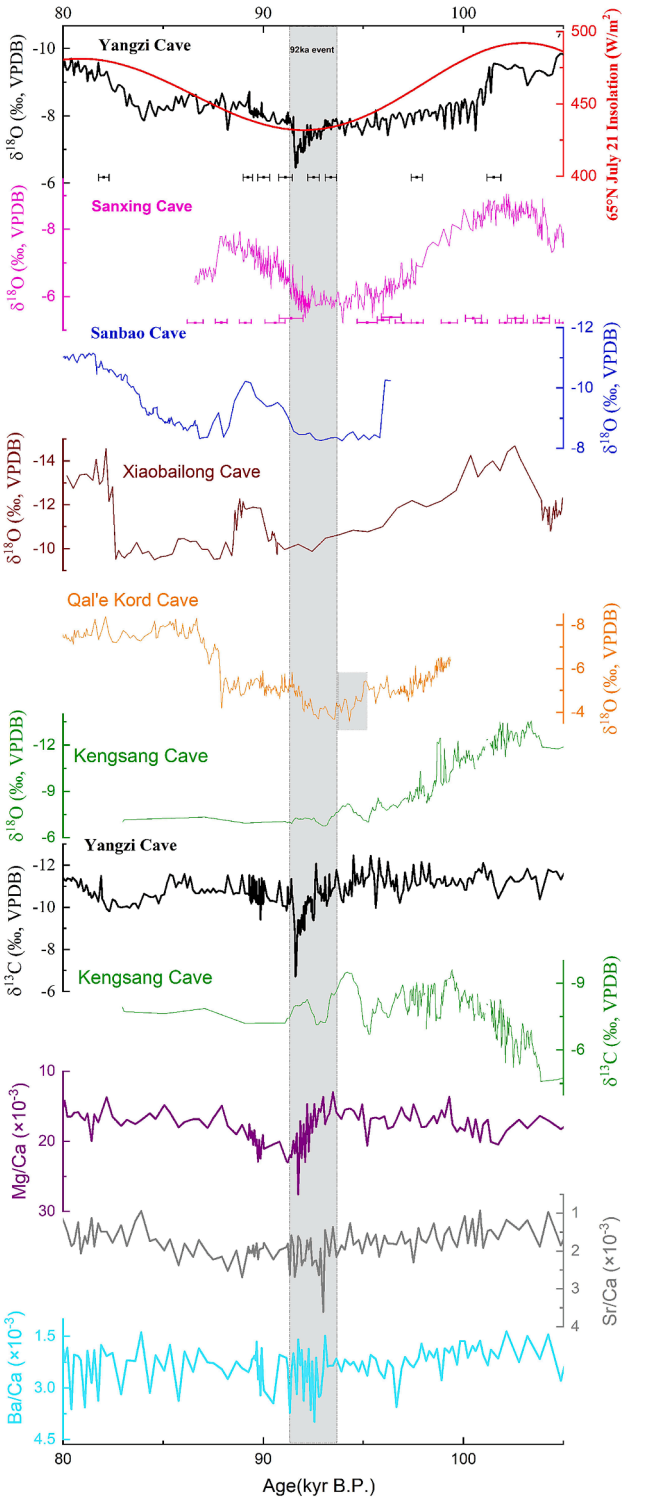

Fig. 7. Comparison of 93.1–91.5 kyr B.P. in stalagmite $\delta^{18}O$, $\delta^{13}C$ records from Yangzi Cave and other records. (a)$\delta^{18}O$ records of stalagmite YYZ1. (b)SX7 from Sanxing Cave (Jiang et al., 2016). (c)SB25–1 from Sanbao Cave(Wang et al., 2008). (d) XBL25 from XiaobailongCave (Cai et al., 2015). (e) QK8 from Qal'ekord Cave (Mehterian et al., 2017). (f)Kesang Cave(green) (Cheng et al., 2012b). (g)$\delta^{13}C$records of stalagmite YYZ1. (h)$\delta^{13}C$ records from Kesang Cave (green) (Cheng et al., 2012b). (e)Mg/Ca ratio of YYZ1 (f)Sr/Ca ratio of YYZ1 (g) Ba/Ca ratio of YYZ1.The gray bar represents the "92kyr event" of weak ASM. (For interpretation of the references to colour in this figure legend, the reader is referred to the web version of this article.)

kyr B.P., which may be similar to that in Kesang Cave, reflects the change in the precipitation source during the weakest period of solar radiation. In contrast, the oxygen isotope record of stalagmite BT2 from Botuvera Cave in the SH exhibited a stable and sustained negative value at 92.7–89.7 kyr B.P. (Fig. 8d). The record of stalagmite DANF from Dante Cave in southern Africa provides more convincing evidence of a wet period at ~92 kyr B.P. These records confirm that the greater solar insolation in the SH brought the tropical rain belt farther south, resulting in increased rainfall (Railsback et al., 2019). Thus, these results indicate that the southward movement of the tropical rainfall belt resulted in more precipitation in the SH low-latitude areas and less precipitation in the NH. The weakening of the summer monsoon and the intensification of local evaporation caused the high $\delta^{18}O$ local water vapour to enter the precipitation clouds. Thereafter, this phenomenon brought about a high $\delta^{18}O$ atmospheric precipitation and ultimately led to a sharp positive shift in the $\delta^{18}O$ values of the speleothems in the NH.

Both the $\delta^{13}C$ and trace element values of stalagmite YYZ1 exhibited positive trends during in this period (Fig. 7). At 92.6 kyr B.P., a rapid decrease in $\delta^{13}C$ leads to a peak of −6.7‰ at 91.6 kyr B.P., and the Mg/Ca curve exhibits similar variations. The Sr/Ca and Ba/Ca ratios exhibited frequent fluctuations and reached their highest values at 93 and 92.5 kyr B.P., respectively. As was previously mentioned, the $\delta^{13}C$ values and trace element ratios of stalagmite YYZ1 mainly reflect the changes in the regional precipitation. During this period, the atmospheric precipitation in the Chongqing area may have mostly originated from local water vapour, the precipitation decreased significantly when the summer monsoon was weak, and the area experienced relatively dry climatic conditions. Long-term drought can change the local vegetation type and density. Due to these changes, the proportion of the C3/C4 vegetation can be reduced and the stalagmite $\delta^{13}C$ values can become positive. Moreover, drier conditions prolong the migration time of karst water, can change its migration path, and can strengthen the PCP effect, causing the $\delta^{13}C$ values of the speleothems to become more positive and increasing the Mg/Ca, Sr/Ca, and Ba/Ca ratios.

In addition, the characteristics of this period have been observed in other geological records. For example, in the Zoige Basin on the eastern edge of the Qinghai-Tibetan Plateau, a low sporopollen concentration occurred in the valley at 92 kyr B.P., indicating a weak summer monsoon period (Shen et al., 2005). The records of the Rb and Sr contents and ratios in the Milanggouwan section of China's Salawusu River Valley confirm that the influence of the winter monsoon was dominant during 92–94 kyr B.P., and the climate was mainly dry and cold at this time (Du et al., 2011). The evidence obtained from numerous geological records leads to the following conclusions. (1) A drought event occurred between 93.1 and 91.5 kyr B.P. At this time, (2) the solar radiation reached the lowest value, (3) the summer monsoon weakened, and (4) the evaporation in the Asian monsoon region was strong. The consistency of these records regarding the occurrence time of the 92 kyr B.P. drought event indicates that the event had a hemispheric effect. However, this inference requires additional higher-resolution records from other regions as support.

4.4. Connection between the ASM and global climate

Seven ASM strengthening events, in concert with D-O events 19–25 in the NGRIP temperature records, were revealed by the negative $\delta^{18}O$in stalagmite YYZ1 record (Fig. 8).Consistently, various geological records have confirmed the coherent millennial-scale variations between the ASM and the climate in the northern hemisphere high latitudes (Yuan et al., 2004; Wang et al., 2008; Cheng et al., 2009; Cai et al., 2010; Cheng et al., 2016a). The temperature changes of the North Atlantic high latitude influence the Asian monsoon via for example, the westerly jet and oceanic belt (Cheng et al., 2012a; Cosford et al., 2008; Chiang et al., 2015; Zhang et al., 2018; Cheng et al., 2020). During MIS 5d and 5b, as the solar radiation initially intensified, plenty of melt water might enter into the Atlantic Ocean, consequently weakening the North Atlantic Deep Water (NADW) and/or THC (Broecker et al., 1992; Bard et al., 2000; Hodell et al., 2017), which is consistent with the ASM weakening recorded by stalagmite YYZ1 records (Fig. 8). During MIS 5c and 5a, the solar radiation was relatively high and a large amount of melt water might also enter into the Atlantic Ocean. However, as the temperature persistently increased, the amount of melt water gradually decreased, which can trigger the rebound of NADW/THC. The changes corresponding to the ASM enhancement were shown in stalagmite YYZ1$\delta^{18}O$ records. Thus, the changes of temperature and ice volume in NH high latitudes might be the important factors of the ASM variations. The changes in the temperature of the North Atlantic can affect the intensity of the Siberian High through the transmission of the westerly belt, and then, they can affect the intensity of the Asian winter monsoon (Porter and An, 1995). The intensity of the summer monsoon weakened while the strength of the winter monsoon increased on millennial timescales (Wen et al., 2016; Kang et al., 2020). The EASM responds to the climate change in the North Atlantic region by rapidly transmitting climate change signals through atmospheric circulation, such as the westerly wind belt, on a wide range of timescales from decades to millennia (Duan et al., 2016; Chiang et al., 2015; Zhang et al., 2018; Cheng et al., 2020). Furthermore, ocean conveyor belts are considered to be the important trigger for global climate changes (Rahmstorf, 2010; Hodell et al., 2017), and it has been profoundly affected by ice-rafted detritus events (IRDs) in the North Atlantic, which means that the massive discharges of the Hudson Strait ice stream drained the Laurentide Ice Sheet (Broecker et al., 1992; Bard et al., 2000; Hodell et al., 2017). Based on the comparison shown in Fig. 8, we detected that IRDs may usually occur at the initial increase or later decrease in the solar radiation intensity.

Although the millennial-scale events (D-O events 19–25) recorded by the $\delta^{18}O$ values of stalagmite YYZ1 are consistent with the NGRIP record, there are differences regarding some details. D-O events 19–25, which were recorded by the NGRIP ice core, were characterized by sudden warming and rapid cooling after maintaining high values for thousands of years (Capron et al., 2010). D-O events 22–25 were clearly shown in the stalagmite YYZ1 $\delta^{18}O$ records, which were characterized by a rapidly decreased $\delta^{18}O$ at the beginning of each event and then slowly approached the maximum within thousands of years. Similar monsoon variations were observed for MIS 2–4 (Duan et al., 2014). However, the process is different from the NGRIP $\delta^{18}O$ record, which abruptly reached the maximum and slowly decreased. Their differences indicate that in addition to climate change in the northern high latitudes, the ASM might be also affected by some other factors, e.g., climate processes in Southern Hemisphere and tropical regions (An et al., 2011; Cai et al., 2010; Cheng et al., 2020). Actually, the millennial-scale events (D-O 20–25) recorded by the $\delta^{18}O$ values of stalagmite YYZ1 are opposite to the millennial-scale events (AIM 20–25) recorded by the $\delta^{18}O$ values of Antarctic ice core EDML. The enhancement (weakening) of the ASM corresponded to a decrease (increase) in the Antarctic temperature (EPICA Community Members, 2006; WAIS, 2015), and the stalagmite $\delta^{18}O$ records in the ASM regions also exhibit an evident antiphase relationship with the $\delta^{18}O$ record of BT2 stalagmite from Botuvera Cave in south-eastern Brazil (Fig. 8e) (Cruz et al., 2009). The $\delta^{18}O$ record in Brazil mainly indicates changes in the locations of the South American summer monsoon (SASM) and the South Atlantic convergence zone (SACZ) (Cruz et al., 2009; Cheng et al., 2013a, 2013b). When the SASM and the SACZ moved northward, the amount of water vapour in the Amazon Basin decreased with the weakening SASM (Wang et al., 2004; Cruz et al., 2009; Cheng et al., 2013a, 2013b). The antiphase relationship between the Asian and South American monsoons supports the centennial-millennial scale seesaw pattern between the two hemispheres (Blunier et al., 1998; Cheng et al., 2012a, 2020). This pattern is mainly related to the intensity of the THC (Rahmstorf, 2002) and the north-south oscillation of the ITCZ (Broccoli et al., 2006; McGee et al., 2014). When the temperature in the SH decreased, the ISM and ASM would be strengthened, accompanied with the northward

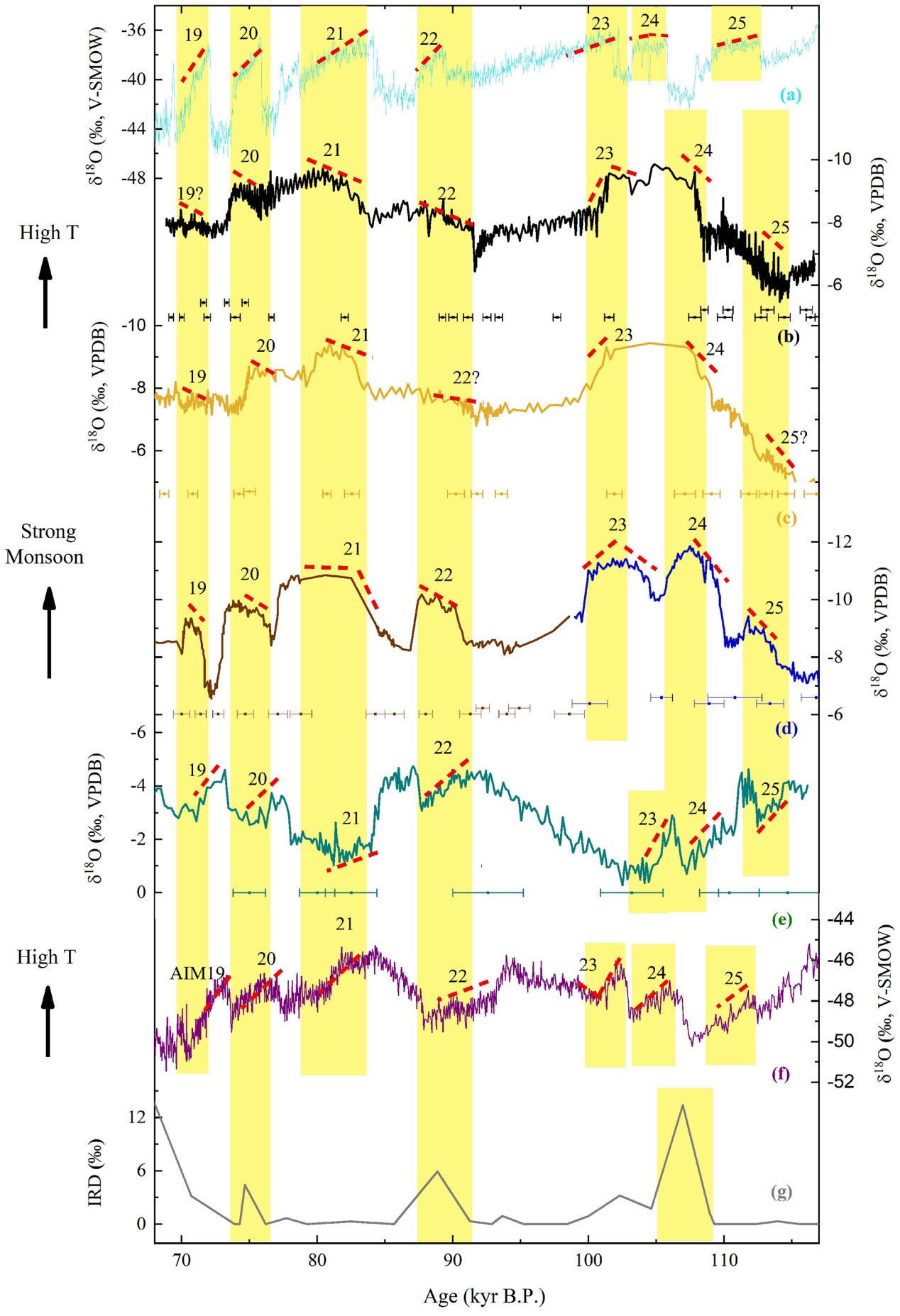

(caption on next page)

Fig. 8. Comparison of stalagmite $\delta^{18}O$ records from Yangzi Cave and other records frommid-high latitude of both hemispheres. (a) NGRIP (AICC2012 time-scale, Veres et al., 2013). (b) $\delta^{18}O$ records of stalagmite YYZ1. (c) YZ1 from Yangzi Cave(Wu et al., 2020). (d)SB22 (pink), SB23 (green) from Sanbao Cave(Wang et al., 2008). (e)BT2 from BotuveraCave (Cruz et al., 2005). (f) Antarctic EDML ice core (EPICA Community Members, 2006). (g)ODP980 IRD (Mcmanus et al., 1999). (For interpretation of the references to colour in this figure legend, the reader is referred to the web version of this article.)

ITCZ, the increased Musklin high pressure, as well as the increased corresponding cross-equatorial airflow and Somali jet (An et al., 2011; Cai et al., 2006). At this time, the SASM and the SACZ also moved northward, and the subtropical summer monsoon precipitation in southeast Brazil decreased, manifested by the enriched $\delta^{18}O$ values of stalagmite BT2. The changes in the temperature of the North Atlantic mainly affect the ASM through the westerly belt and the ocean conveyor belt in the northern high latitudes (Chiang et al., 2015; Zhang et al., 2018; Cheng et al., 2020), while low-latitude processes that forcing of ASM variations likely influenced by the variations of the western Pacific subtropical high, ITCZ, and the Hadley circulation (Tan, 2014; Zhao et al., 2019; Cheng et al., 2020).

5. Conclusions

The high-resolution palaeoclimatic records during the 117–69 kyr B.P. period in Chongqing were reconstructed based on the oxygen and carbon isotopes and trace elements of speleothem YYZ1 from Yangzi cave and U-Th dating. The $\delta^{18}O$ values of stalagmite YYZ1 recorded millennial-scale D-O events 19–25, which occurred during MIS 5, but D-O event 19 was not distinct. We conclude that the $\delta^{18}O$ values of stalagmite YYZ1 reflect the variation in the intensity of the summer monsoon, and the range of the $\delta^{18}O$ values is basically consistent with the solar radiation energy curve for 65°N. This indicates that the variation in the ASM intensity was mainly controlled by the external astronomical orbital parameters on the orbital scale during this period, and it exhibited obvious precession cycle fluctuation characteristics. The $\delta^{13}C$ values were negative when the summer monsoon was strong (MIS 5c and 5a) and were positive when it was weak (MIS 5d, 5b, and 4), corresponding to the variations in the Mg/Ca, Sr/Ca, and Ba/Ca ratios and reflecting the dry or wet conditions outside the local area and the hydrological processes and biological activity.

Based on the multi-proxy records for 93.1–91.5 kyr B.P., a drought event occurred due to the influences of biological activity and predominantly the monsoon intensity and precipitation. The comparison of the NGRIP ice core and the stalagmite records from the Asian monsoon region indicate the existence of the D-O 25 event and events similar to the D-O 25 event in the stalagmite $\delta^{18}O$ records from the Asian monsoon region. Moreover, their amplitudes are significantly weaker than those of the other centennial-millennial scale climate events. We concluded that the millennial-scale events during the interglacial periods were triggered by processes in the NH low latitudes and were dominant factors affecting the monsoon circulation and the climate change in the SH. This may be a very complicated and challenging research field, but it can be crucial to understand orbital-millennial-scale climate changes and the relationship between low latitude processes and global changes. Our research also reflects information about climate change in the North Atlantic and clearly demonstrates the seesaw effect in the SH records. This illustrates the coupling between the climate at high latitudes and the processes in the Northern Hemisphere and between the climate at low latitudes and the processes in the Southern Hemisphere.

Funding

This work was supported by grants from the National Natural Science Foundation of China (grant number 41877450 and 41672160) to Y. Yang; and the National Natural Science Foundation of China (grant number 41772170) to T.-Y. Li.

Declaration of Competing Interest

The authors declare that they have no known competing financial interests or personal relationships that could have appeared to influence the work reported in this paper.

Appendix A. Supplementary data

Supplementary data to this article can be found online at https://doi.org/10.1016/j.palaeo.2021.110798.

References

An, Z.S., Clemens, S.C., Shen, J., Qiang, X.K., Jin, Z.D., Sun, Y.B., Prell, W.L., Luo, J.J., Wang, S.M., Xu, H., Cai, Y.J., Zhou, W.J., Liu, X.D., Liu, W.G., Shi, Z.G., Yan, L.B., Xiao, X.Y., Chang, H., Wu, F., Ai, L., Lu, F.Y., 2011. Glacial-interglacial indian summer monsoon dynamics. Science 333, 719–723.

Andersen, K.K., Azuma, N., Barnola, J.M., Bigler, M., Biscaye, P., Caillon, N., Chappellaz, J., Clausen, H.B., DahlJensen, D., Fischer, H., Fluckiger, J., Fritzsche, D., Fujii, Y., Goto-Azuma, K., Gronvold, K., Gundestrup, N.S., Hansson, M., Huber, C., Hvidberg, C.S., Johnsen, S.J., Jonsell, U., Jouzel, J., Kipfstuhl, S., Landais, A., Leuenberger, M., Lorrain, R., Masson-Delmotte, V., Miller, H., Motoyama, H., Narita, H., Popp, T., Rasmussen, S.O., Raynaud, D., Rothlisberger, R., Ruth, U., Samyn, D., Schwander, J., Shoji, H., Siggard-Andersen, M.L., Steffensen, J.P., Stocker, T., Sveinbjornsdottir, A.E., Svensson, A., Takata, M., Tison, J.L., Thorsteinsson, T., Watanabe, O., Wilhelms, F., White, J.W.C., Project, N.G.I.C, 2004. High-resolution record of Northern Hemisphere climate extending into the last interglacial period. Nature 431, 147–151.

Baker, A., Ito, E., Smart, P.L., McEwan, R.F, 1997. Elevated and variable values of ^{13}C in speleothems in a British cave system. Chem. Geol. 136, 263–270.

Bakker, P., Clark, P.U., Golledge, N.R., Schmittner, A., Weber, M.E., 2017. Centennial-scale Holocene climate variations amplified by Antarctic Ice Sheet discharge. Nature 541, 72.

Bard, E., Rostek, F., Turon, J.L., Gendreau, S., 2000. Hydrologicalimpact of Heinrich events in the subtropical northeast Atlantic. Science 289, 1321–1324.

Bar-Matthews, M., Ayalon, A., Kaufman, A., 2000. Timing and hydrological conditions of Sapropel events in the Eastern Mediterranean, as evident from speleothems, Soreq cave, Israel. ChemGeol 169, 145–156.

Beck, J.W., Zhou, W.J., Li, C., Wu, Z.K., White, L., Xian, F., Kong, X.H., An, Z., 2018. A 550,000-year record of East Asian monsoon rainfall from Be-10 in loess. Science 360, 877.

Blunier, T., Chappellaz, J., Schwander, J., Dällenbach, A., Stauffer, B., Stocker, T.F., Raynaud, D., Jouzel, J., Clausen, H.B., Hammer, C.U., Johnsen, S.J., 1998. Asynchrony of Antarctic and Greenland climate change during the last glacial period. Nature 394, 739–743.

Boch, R., Cheng, H., Spötl, C., Edwards, R.L., Wang, X., Hauselmann, P., 2011. NALPS: a precisely dated European climate record 120-60 ka. Clim. Past 7, 1247–1259.

Breitenbach, S.F.M., Rehfeld, K., Goswami, B., Baldini, J.U.L., Ridley, H.E., Kennett, D.J., Prufer, K.M., Aquino, V.V., Asmerom, Y., Polyak, V.J., Cheng, H., Kurths, J., Marwan, N., 2012. COnstructing Proxy Records from Age models (COPRA). Clim. Past 8, 1765–1779.

Broccoli, A.J., Dahl, K.A., Stouffer, R.J., 2006. Response of the ITCZ to Northern Hemisphere cooling. Geophys. Res. Lett. 33.

Broecker, W.S., 1998. Paleocean circulation during the last deglaciation: a bipolar seesaw? Paleoceanography 13, 119–121.

Broecker, W.S., Bond, G., Klas, M., Clark, E., McManus, J., 1992. Origin of the northern Atlantic's Heinrich events. Clim. Dyn. 6, 265–273.

Cai, Y.J., An, Z.S., Cheng, H., Edwards, R.L., Kelly, M.J., Liu, W.G., Wang, X.F., Shen, C. C., 2006. High-resolution absolute-dated Indian Monsoon record between 53 and 36 ka from Xiaobailong Cave, southwestern China. Geology 34, 621–624.

Cai, Y.J., Cheng, H., An, Z.S., Edwards, R.L., Wang, X.F., Tan, L.C., Wang, J., 2010. Large variations of oxygen isotopes in precipitation over south-Central Tibet during Marine Isotope Stage 5. Geology 38, 243–246.

Cai, Y.J., Fung, I.Y., Edwards, R.L., An, Z.S., Cheng, H., Lee, J-E., Tan, L.C., Shen, C.-C., Wang, X.F., Day, J.A., Zhou, W.J., Kelly, M.J., Chiang, J.C.H., 2015. Variability of stalagmite-inferred Indian monsoon precipitation over the past 252,000 year. Proc. Natl. Academy Sci. 112, 2954–2959.

Caley, T., Roche, D.M., Renssen, H., 2014. Orbital Asian summer monsoon dynamics revealed using an isotope- enabled global climate model. Nat. Commun. 5.

Capron, E., Landais, A., Chappellaz, J., Schilt, A., Buiron, D., Dahl-Jensen, D., Johnsen, S. J., Jouzel, J., Lemieux-Dudon, B., Loulergue, L., Leuenberger, M., Masson-Delmotte, V., Meyer, H., Oerter, H., Stenni, B., 2010. Millennial and sub-millennial scale climatic variations recorded in polar ice cores over the last glacial period. Clim. Past 6, 345–365.

Capron, E., Landais, A., Chappellaz, J., Buiron, D., Fischer, H., Johnsen, S.J., Jouzel, J., Leuenberger, M., Masson-Delmotte, V., Stocker, T.F., 2012. A global picture of the first abrupt climatic event occurring during the last glacial inception. Geophys. Res. Lett. 39.
Cheng, H., Edwards, R.L., Hoff, J., Gallup, C.D., Richards, D.A., Asmerom, Y., 2000. The half-lives of uranium-234 and thorium-230. Chem. Geol. 169, 17–33.
Cheng, H., Edwards, R.L., Wan, Y.J., Ko, X.G., Ming, Y.F., Kelly, M.J., Wang, X.F., Gallup, C.D., Liu, W.G., 2006. A penultimate glacial monsoon record from Hulu Cave and two-phase glacial terminations. Geology 34, 217–220.
Cheng, H., Edwards, R.L., Broecker, W.S., Denton, G.H., Kong, X.G., Wang, Y.J., Zhang, R., Wang, X.F., 2009. Ice age terminations. Science 326, 248–252.
Cheng, H., Sinha, A., Wang, X.F., Cruz, F.W., Edwards, R.L., 2012a. The Global Paleomonsoon as seen through speleothem records from Asia and the Americas. Clim.Dyn. 39, 1045–1062.
Cheng, H., Zhang, P.Z., Spötl, C., Edwards, R.L., Cai, Y.J., Zhang, D.Z., Sang, W.C., Tan, M., An, Z.S., 2012b. The climatic cyclicity in semiarid-arid Central Asia over the past 500,000 years. Geophys. Res. Lett. 39, L01705.
Cheng, H., Edwards, R.L., Shen, C.C., Polyak, V.J., Asmerom, Y., Woodhead, J., Hellstrom, J., Wang, Y.J., Kong, X.G., Spötl, C., Wang, X.F., Alexander, E.C., 2013a. Improvements in Th-230 dating, Th-230 and U-234 half-life values, and U-Th isotopic measurements by multi-collector inductively coupled plasma mass spectrometry. Earth Planet. Sci. Lett. 371, 82–91.
Cheng, H., Sinha, A., Cruz, F.W., Wang, X.F., Edwards, R.L., d'Horta, F.M., Ribas, C.C., Vuille, M., Stott, L.D., Auler, A.S., 2013b. Climate change patterns in Amazonia and biodiversity. Nat. Commun. 4 (1), 1–6.
Cheng, H., Edwards, R.L., Sinha, A., Spötl, C., Yi, L., Chen, S.T., Kelly, M., Kathayat, G., Wang, X.F., Li, X.L., Kong, X.G., Wang, Y.J., Ning, Y.F., Zhang, H.W., 2016a. The Asian monsoon over the past 640,000 years and ice age terminations. Nature 534, 640.
Cheng, H., Spötl, C., Breitenbach, S.F.M., Sinha, A., Wassenburg, J.A., Jochum, K.P., Scholz, D., Li, X.L., Yi, L., Peng, Y.B., Lv, Y.B., Zhang, P.Z., Votintseva, A., Loginov, V., Ning, Y.F., Kathayat, G., Edwards, R.L., 2016b. Climate variations of Central Asia on orbital to millennial timescales. Sci Rep-Uk 6, 36975.
Cheng, H., Zhang, H.W., Zhao, J.Y., Li, H.Y., Ning, Y.F., Kathayat, G., 2019. Chinese stalagmite paleoclimate researches: a review and perspective. Science China-Earth Sci. 62, 1489–1513.
Cheng, H., Zhang, H., Spotl, C., Baker, J., Sinha, A., Li, H., Bartolome, M., Moreno, A., Kathayat, G., Zhao, J., Dong, X., Li, Y., Ning, Y., Jia, X., Zong, B., AitBrahim, Y., Perez-Mejias, C., Cai, Y., Novello, V.F., Cruz, F.W., Severinghaus, J.P., An, Z., Edwards, R.L., 2020. Timing and Structure of the Younger Dryas Event and its Underlying Climate Dynamics, PNAS117, pp. 23408–23417.
Chiang, J.C.H., Fung, I.Y., Wu, C.H., Cai, Y., Labrousse, C.A., 2015. Role of seasonal transitions and westerly jets in East Asian paleoclimate. Quat. Sci. Rev. 108, 111–129.
Columbu, A., Spötl, C., De Waele, J., Yu, T.L., Shen, C.C., Gazquez, F., 2019. A long record of MIS 7 and MIS 5 climate and environment from a western Mediterranean speleothem (SW Sardinia, Italy). Quat. Sci. Rev. 220, 230–243.
Cosford, J., Qing, H.R., Eglington, B., Mattey, D., Yuan, D.X., Zhang, M.L., Cheng, H., 2008. East Asian monsoon variability since the Mid-Holocene recorded in a high-resolution, absolute-dated aragonite speleothem from eastern China. Earth Planet. Sci. Lett. 275, 296–307.
Cruz, F.W., Burns, S.J., Jercinovic, M., Karmann, I., Sharp, W.D., Vuille, M., 2007. Evidence of rainfall variations in Southern Brazil from trace element ratios (Mg/Ca and Sr/Ca) in a late Pleistocene stalagmite. Geochim.Cosmochim.Acta 71, 2250–2263.
Cruz, F.W., Burns, S.J., Karmann, I., Sharp, W.D., Vuille, M., Cardoso, A.O., Ferrari, J.A., Dias, P.L.S., Viana, O., 2005. Insolation-driven changes in atmospheric circulation over the past 116,000 years in subtropical Brazil. Nature 434, 63–66.
Cruz, F.W., Vuille, M., Burns, S.J., Wang, X.F., Cheng, H., Werner, M., Edwards, R.L., Karmann, I., Auler, A.S., Nguyen, H., 2009. Orbitally driven east–west antiphasing of South American precipitation. Nat. Geosci. 2 (3), 210–214.
Dansgaard, W., Johnsen, S.J., Clausen, H.B., Dahljensen, D., Gundestrup, N.S., Hammer, C.U., Hvidberg, C.S., Steffensen, J.P., Sveinbjornsdottir, A.E., Jouzel, J., Bond, G., 1993. Evidence for general instability of past climate from a 250-Kyr ice-core record. Nature 364, 218–220.
Ding, Y.H., Li, C.Y., Liu, Y.J., 2004. Overview of the South China Sea monsoon experiment. Adv. Atmos. Sci. 21, 343–360.
Dong, J., Kan, Z., Shen, C.C., Ren, H., 2016. Strong East Asian summer monsoon during the DO 25 event recorded by an absolute-dated stalagmite from Dragon Cave, Northern China. Quat. Sci. 36, 1502–1509 (in Chinese with English abstract).
Dorale, J.A., Edwards, R.L., Ito, E., Gonzalez, L.A., 1998. Climate and vegetation history of the midcontinent from 75 to 25 ka: a speleothem record from Crevice Cave, Missouri, USA. Science 282, 1871–1874.
Drumond, A., Nieto, R., Gimeno, L., 2011. Sources of moisture for China and their variations during drier and wetter conditions in 2000-2004: a Lagrangian approach. Clim. Res. 50, 215–225.
Drysdale, R.N., Zanchetta, G., Hellstrom, J.C., Fallick, A.E., McDonald, J., Cartwright, I., 2007. Stalagmite evidence for the precise timing of North Atlantic cold events during the early last glacial. Geology 35, 77–80.
Du, S.H., Li, B.S., Niu, D.F., Zhang, D.D., Wen, X.H., Chen, D.N., Yang, Y., Wang, F.N., 2011. Age of the MGS5 segment of the Milanggouwanstratigraphical section and evolution of the desert environment on a kiloyear scale during the last Interglacial in China's Salawusu River Valley: evidence from Rb and Sr contents and ratios. Chem. Erde-Geochem. 71, 87–95.
Du, W.J., Cheng, H., Xu, Y., Yang, X.L., Zhang, P.Z., Sha, L.J., Li, H.Y., Zhu, X.Y., Zhang, M.L., Strikis, N.M., Cruz, F.W., Edwards, R.L., Zhang, H.W., Ning, Y.F., 2019. Timing and structure of the weak Asian Monsoon event about 73,000 years ago. Quat.Geochro 53.
Duan, W.H, Ruan, J.Y., Luo, W.J., Li, T-Y., Tian, L.J., Zeng, G.N., Zhang, D.Z., Bai, Y.J., Li, J.L., Tao, T., Zhang, P.Z., Tan, M., 2016. The transfer of seasonal isotopic variability between precipitation and drip water at eight caves in the monsoon regions of China. Geochim. Cosmochim. Acta 183, 250–266.
Duan, F.C., Wang, Y.J., Shen, C.C., Wang, Y., Cheng, H., Wu, C.C., Hu, H.M., Kong, X.G., Liu, D.B., Zhao, K., 2014. Evidence for solar cycles in a late Holocene speleothem record from Dongge Cave. China. Sci Rep-Uk 4.
Duan, W.H., Cheng, H., Tan, M., Edwards, R.L., 2016. Onset and duration of transitions into Greenland Interstadials 15.2 and 14 in northern China constrained by an annually laminated stalagmite. Sci Rep-Uk 6.
Fairchild, I.J., Treble, P.C., 2009. Trace elements in speleothems as recorders of environmental change. Quat. Sci. Rev. 28, 449–468.
Fairchild, I.J., Borsato, A., Tooth, A.F., Frisia, S., Hawkesworth, C.J., Huang, Y.M., McDermott, F., Spiro, B., 2000. Controls on trace element (Sr-Mg) compositions of carbonate cave waters: implications for speleothem climatic records. Chem. Geol. 166, 255–269.
EPICA Community Members, 2006. One-to-one coupling of glacial climate variability in Greenland and Antarctica. Nature 444, 195–198.
Fairchild, I.J., Baker, A., Borsato, A., Frisia, S., Hinton, R.W., McDermott, F., Tooth, A.F., 2001. Annual to sub-annual resolution of multiple trace-element trends in speleothems. J. Geol. Soc. Lond. 158, 831–841.
Fohlmeister, J., Voarintsoa, N.R.G., Lechleitner, F.A., Boyd, M., Brandtstätter, S., Jacobson, M.J., Oster, J.L., 2020. Main controls on the stable carbon isotope composition of speleothems. Geochim. Cosmochim. Acta 279, 67–87.
Galaasen, E.V., Ninnemann, U.S., Irvali, N., Kleiven, H.F., Rosenthal, Y., Kissel, C., Hodell, D.A., 2014. Rapid reductions in North Atlantic deep water during the peak of the last interglacial period. Science 343, 1129–1132.
Genty, D., Blamart, D., Ouahdi, R., Gilmour, M., Baker, A., Jouzel, J., Van-Exter, S., 2003. Precise dating of Dansgaard-Oeschger climate oscillations in western Europe from stalagmite data. Nature 421, 833–837.
Heinrich, H., 1988. Origin and consequences of cyclic ice rafting in the Northeast Atlantic-Ocean during the past 130,000 years. Quat. Res. 29, 142–152.
Hellstrom, J.C., Mcculloch, M.T., 2000. Multi-proxy constraints on the climatic significance of trace element records from a New Zealand speleothem. Earth Planet. Sc. Lett. 179, 287–297.
Hendy, C.H., 1971. The isotopic geochemistry of speleothems—I. the calculation of the effects of different modes of formation on the isotopic composition of speleothems and their applicability as palaeoclimatic indicators. Geochim.Cosmochim.Acta 35, 801–824.
Hodell, D.A., Nicholl, J.A., Bontognali, T.R.R., Danino, S., Dorador, J., Dowdeswell, J.A., Einsle, J., 2017. Anatomy ofHeinrich Layer 1 and its role in the last deglaciation. Paleoceanography 32, 284–303.
Jahn, B-M., Gallet, S., Han, J.M., 2001. Geochemistry of the Xining, Xifeng and Jixian sections, Loess Plateau of China: Eolian dust provenance and paleosol evolution during the last 140 ka. Chem. Geol. 178, 71–94.
Jiang, X.Y., Wang, X.Y., He, Y.Q., Hu, H.M., Li, Z.Z., Spötl, C., Shen, C.C., 2016. Precisely dated multidecadally resolved Asian summer monsoon dynamics 113.5-86.6 thousand years ago. Quat. Sci. Rev. 143, 1–12.
Johnson, K.R., Hu, C.Y., Belshaw, N.S., Henderson, G.M., 2006a. Seasonal trace-element and stable-isotope variations in a Chinese speleothem: the potential for high-resolution paleomonsoon reconstruction. EarthPlanet. Sci. Lett. 244, 394–407.
Johnson, K.R., Ingram, B.L., Sharp, W.D., Zhang, P.Z., 2006b. East Asian summer monsoon variability during Marine Isotope Stage 5 based on speleothem delta O-18 records from Wanxiang Cave, central China. Palaeogeogr. Palaeoclimatol. Palaeoecol. 236, 5–19.
Kang, S., Du, J., Wang, N., Dong, J.B., Wang, D., Wang, X.L., Qiang, X.K., Song, Y.G., 2020. Early Holocene weakening and mid-to late Holocene strengthening of the East Asian winter monsoon. Geology 48 (11), 1043–1047.
Kelly, M.J., Edwards, R.L., Cheng, H., Yuan, D.X., Cai, Y.J., Zhang, M.L., Lin, Y.S., An, Z. S., 2006. High resolution characterization of the Asian Monsoon between 146,000 and 99,000 years BP from Dongge Cave, China and global correlation of events surrounding termination II. Palaeogeogr.Palaeoclimatol.Palaeoecol. 236, 20–38.
Li, H.C., Ku, T.L., You, C.F., Cheng, H., Edwards, R.L., Ma, Z.B., Tsai, W.S., Li, M.D., 2005. Sr-87/Sr-86 and Sr/Ca in speleothems for paleoclimate reconstruction in Central China between 70 and 280 kyr ago. Geochim.CosmochimActa 69, 3933–3947.
Li, T.-Y., Shen, C.C., Huang, L.J., Jiang, X.Y., Yang, X.L., Mii, H.S., Lee, S.Y., Lo, L., 2014. Stalagmite-inferred variability of the Asian summer monsoon during the penultimate glacial–interglacial period. Clim. Past 10, 1211–1219.
Li, T.-Y., Huang, C.-X., Tian, L., Suaraz, M.B., Gao, Y., 2018. Variation of $\delta^{13}C$ in plant-soil-cave systems in karst regions with different degrees of rocky desertification in Southwest China and implications for paleoenvironment reconstruction. J. Cave Karst Stud. 80 (4), 212–228.
Liu, Z., Wen, X., Brady, E.C., Otto-Bliesner, B., Yu, G., Lu, H., Cheng, H., Wang, Y., Zheng, W., Ding, Y., Edwards, R.L., Cheng, J., Liu, W., Yang, H., 2014. Chinese cave records and the East Asia Summer Monsoon. Quat. Sci. Rev. 83, 115–128.
Liu, X., Liu, J., Chen, S., Chen, J., Zhang, X., Yan, J., Chen, F., 2020. New insights on Chinese cave $\delta^{18}O$ records and their paleoclimatic significance. ESR 103216.
Lohmann, J., Ditlevsen, P.D., 2019. Objective extraction and analysis of statistical features of Dansgaard-Oeschger events. Clim. Past 15 (5), 1771–1792.
Lüthi, D., Le Floch, M., Bereiter, B. Blunier, Barnola, J.-M., Siegenthaler, U., Raynaud, D., Jouzel, J., Fischer, H., Kawamura, K., Stocker, T.F., 2008. High-resolution carbon dioxide concentration record 650,000-800,000 years before present. Nature 453, 379–382.

McDermott, F., 2004. Palaeo-climate reconstruction from stable isotope variations in speleothems: a review. Quat. Sci. Rev. 23, 901–918.
McGee, D., Donohoe, A., Marshall, J., Ferreira, D., 2014. Changes in ITCZ location and cross-equatorial heat transport at the last Glacial Maximum, Heinrich Stadial 1, and the mid-Holocene. Earth Planet. Sci. Lett. 390, 69–79.
Mcmanus, J.F., Oppo, D.W., Cullen, J.L., 1999. A 0.5-million-year record of millennial-scale climate variability in the north Atlantic. Science 283, 971–975.
Mehterian, S., Pourmand, A., Sharifi, A., Lahijani, H.A.K., Naderi, M., Swart, P.K., 2017. Speleothem records of glacial/interglacial climate from Iran forewarn of future water availability in the interior of the Middle East. Quat. Sci. Rev. 164, 187–198.
Nehme, C., Verheyden, S., Noble, S.R., Farrant, A.R., Sahy, D., Hellstrom, J., Delannoy, J. J., Claeys, P., 2015. Reconstruction of MIS 5 climate in the central Levant using a stalagmite from Kanaan Cave. Lebanon. Clim. Past. 11, 1785–1799.
North Greenland Ice Core Project Members, 2004. High-resolution record of northern hemisphere climate extending into the last interglacial period. Nature 431, 147–151.
Oneil, J.R., Clayton, R.N., Mayeda, T.K., 1969. Oxygen isotope fractionation in divalent metal carbonates. J. Chem. Phys. 51, 5547–5558.
Oppo, D.W., McManus, J.F., Cullen, J.L., 2006. Evolution and demise of the last Interglacial warmth in the subpolar North Atlantic. Quat. Sci. Rev. 25, 3268–3277.
Petit, J.R., Jouzel, J., Raynaud, D., Barkov, N.I., Barnola, J.M., Basile, I., Bender, M., Chappellaz, J., Davis, M., Delaygue, G., Delmotte, M., Kotlyakov, V.M., Legrand, M., Lipenkov, V.Y., Lorius, C., Pepin, L., Ritz, C., Saltzman, E., Stievenard, M., 1999. Climate and atmospheric history of the past 420,000 years from the Vostok ice core, Antarctica. Nature 399, 429–436.
Plagnes, V., Causse, C., Dominique, G., Paterne, M., Blamart, D., 2002. A discontinuous climatic record from 187 to 74 ka from a speleothem of the Clamouse Cave (south of France). EarthPlanet. Sci. Lett. 201, 87–103.
Porter, S.C., An, Z.S., 1995. Correlation between climate events in the North-Atlantic and China during last glaciation. Nature 375, 305–308.
Qin, J.M., Yuan, D.X., Cheng, H., Lin, Y.S., Zhang, M.L., 2004. The Stable isotope and trace element records on environmental change of D3 stalagmite in Dongge Cave, Libo, Guizhou. Acta Geoscientica Sinica 25, 625–632. (in Chinese with English abstract).
Rahmstorf, S., 2002. Ocean circulation and climate during the past 120,000 years. Nature 419, 207–214.
Rahmstorf, S., 2010. How ocean stirring affects climate. Nature 464, 681.
Railsback, L.B., Kraft, S., Liang, F.Y., Brook, G.A., Marais, E., Cheng, H., Edwards, R.L., 2019. Control of insolation on stalagmite growth, rainfall, and migration of the tropical rain belt in northern Namibia over the last 100 kyr, as suggested by a rare MIS 5b-5c stalagmite from Dante Cave. Palaeogeogr. Palaeoclimatol. Palaeoecol. 535, 109348.
Rama-Corredor, O., Martrat, B., Grimalt, J.O., Lopez-Otalvaro, G.E., Flores, J.A., Sierro, F., 2015. Parallelisms between sea surface temperature changes in the western tropical Atlantic (Guiana Basin) and high latitude climate signals over the last 140 000 years. Clim. Past 11, 1297–1311.
Rossi, C., Mertz-Kraus, R., Osete, M.L., 2014. Paleoclimate variability during the Blake geomagnetic excursion (MIS 5d) deduced from a speleothem record. Quat. Sci. Rev. 102, 166–180.
Ruan, J.Y., Zhang, H.Y, Cai, Z.Y., Yang, X.Q., Yin, J., 2019. Regional controls on daily to interannual variations of precipitation isotope ratios in Southeast China: Implications for paleomonsoon reconstruction. Earth Planet. Sc. Lett. 527, 115794.
Shackleton, N.J., 1987. Oxygen isotopes, ice volume and sea level. Quat. Sci. Rev. 6, 183–190.
Shen, C.C., Edwards, R.L., Cheng, H., Dorale, J.A., Thomas, R.B., Moran, S.B., Weinstein, S.E., Edmonds, H.N., 2002. Uranium and thorium isotopic and concentration measurements by magnetic sector inductively coupled plasma mass spectrometry. Chem. Geol. 185, 165–178.
Shen, C.M., Tang, L.Y., Wang, S.M., Li, C.H., Liu, K.B., 2005. Pollen records and time scale for the RM core of the Zoige Basin, northeastern Qinghai-Tibetan Plateau. Chin. Sci. Bull. 50, 553–562 (in Chinese with English abstract).
Tan, M., 2014. Circulation effect: response of precipitation $\delta^{18}O$ to the ENSO cycle in monsoon regions of China. Clim.Dyn. 42, 1067–1077.
Tan, L.C., Cai, Y.J., Cheng, H., An, Z.S., Edwards, R.L., 2009. Summer monsoon precipitation variations in Central China over the past 750 years derived from a high-resolution absolute-dated stalagmite. Palaeogeogr.Palaeoclimatol.Palaeoecol. 280, 432–439.
Treble, P., Shelley, J.M.G., Chappell, J., 2003. Comparison of high resolution sub-annual records of trace elements in a modern (1911-1992) speleothem with instrumental climate data from southwest Australia. Earth Planet. Sc. Lett. 216, 141–153.
Veres, D., Bazin, L., Landais, A., Kele, H.T.M., Lemieux-Dudon, B., Parrenin, F., Martinerie, P., Blayo, E., Blunier, T., Capron, E., Chappellaz, J., Rasmussen, S.O., Severi, M., Svensson, A., Vinther, B., Wolff, E.W., 2013. The Antarctic ice core chronology (AICC2012): an optimized multi-parameter and multi-site dating approach for the last 120 thousand years. Clim. Past 9, 1733–1748.
Verheyden, S., Keppens, E., Fairchild, I.J., McDermott, F., Weis, D., 2000. Mg, Sr and Sr isotope geochemistry of a Belgian Holocene speleothem: implications for paleoclimate reconstructions. Chem. Geol. 169, 131–144.
WAIS Divide Project Members, 2015. Precise interpolar phasing of abrupt climate change during the last ice age. Nature 520 (7549), 661–665.
Wang, Y.J., Cheng, H., Edwards, R.L., An, Z.S., Wu, J.Y., Shen, C.C., Dorale, J.A., 2001. A high-resolution absolute-dated late Pleistocene monsoon record from Hulu Cave, China. Science 294, 2345–2348.
Wang, P.X., 2006. Orbital forcing of the low-latitude processes. Quat. Sci. 5, 694–701. (in Chinese with English abstract).
Wang, X.F., Auler, A.S., Edwards, R.L., Cheng, H., Cristalli, P.S., Smart, P.L., Richards, D. A., Shen, C.C., 2004. Wet periods in northeastern Brazil over the past 210 kyr linked to distant climate anomalies. Nature 432, 740–743.
Wang, Y.J., Cheng, H., Edwards, R.L., Kong, X.G., Shao, X.H., Chen, S.T., Wu, J.Y., Jiang, X.Y., Wang, X.F., An, Z.S., 2008. Millennial- and orbital-scale changes in the East Asian monsoon over the past 224,000 years. Nature 451, 1090–1093.
Wen, X., Liu, Z., Wang, S., Cheng, J., Zhu, J., 2016. Correlation and anti-correlation of the East Asian summer and winter monsoons during the last 21,000 years. Nat. Commun. 7, 11999.
Wu, S., Chen, S., Duan, F., 2012. The Relation between the 72 ka event and the Toba Super-eruption. Adv. Earth Science 27, 35–41.
Wu, Y., Li, T.-Y., Yu, T.L., Shen, C.C., Chen, C.-J., Zhang, J., Li, J.Y., Wang, T., Huang, R., Xiao, S.Y., 2020. Variation of the Asian summer monsoon since the last glacial-interglacial recorded in a stalagmite from Southwest China. Quat. Sci. Rev. 234, 106261.
Yuan, D.X., Cheng, H., Edwards, R.L., Dykoski, C.A., Kelly, M.J., Zhang, M.L., Qing, J.M., Lin, Y.S., Wang, Y.J., Wu, J.Y., Dorale, J.A., An, Z.S., Cai, Y.J., 2004. Timing, duration, and transitions of the last Interglacial Asian Monsoon. Science 304, 575–578.
Zhang, J., Li, T.-Y., 2019. Seasonal and interannual variations of hydrochemical characteristics and stable isotopic compositions of drip waters in Furong Cave, Southwest China based on 12 years' monitoring. J.Hydrol. 572, 40–50.
Zhang, T.T., Li, T.-Y., Cheng, H., Edwards, R.L., Shen, C.C., Spötl, C., Li, H.C., Han, L.Y., Li, J.Y., Huang, C.X., Zhao, X., 2017. Stalagmite-inferred centennial variability of the Asian summer monsoon in Southwest China between 58 and 79 ka BP. Quat. Sci. Rev. 160, 1–12.
Zhang, H.B., Griffiths, M.L., Chiang, J.C.H., Kong, W.W., Wu, S.T., Atwood, A., Huang, J. H., Cheng, H., Ning, Y.F., Xie, S.C., 2018. East Asian hydroclimatemodulated by the position of the westerlies during termination I. Science 362, 580–583.
Zhao, J., Cheng, H., Yang, Y., Tan, L.C., Spötl, C., Ning, Y.F., Zhang, H.W., Cheng, X., Sun, Z., Li, X.L., Li, H.Y., Liu, W., Edwards, R.L., 2019. Reconstructing the Western boundary variability of the Western Pacific Subtropical High over the past 200 years via Chinese cave oxygen isotope records. Clim.Dyn. 52 (5), 3741–3757.
Zhou, H.Y., Wang, Y., Huang, L.Y., Mai, S.Q., 2011. Speleothem Mg, Sr and Ba records during the MIS 5c-d, and implications for paleoclimate change in NE Sichuan, Central China. Chinese Sci. Bull. 56, 3445–3450.
Zhou, H.Y., Zhao, J.X., Zhang, P.Z., Shen, C.C., Chi, B.Q., Feng, Y.X., Lin, Y., Guan, H.Z., You, C.F., 2008. Decoupling of stalagmite-derived Asian summer monsoon records from North Atlantic temperature change during marine oxygen isotope stage 5d. Quat. Res. 70, 315–321.
Zhou, H.Y., Feng, Y.X., Zhao, J.X., Shen, C.C., You, C.F., Lin, Y., 2009. Deglacial variations of Sr and Sr-87/Sr-86 ratio recorded by a stalagmite from Central China and their association with past climate and environment. Chem. Geol. 268, 233–247.
Zhu, X.W., Zhang, Y.H., Han, D.S., Wen, R.P., Chen, B.Q., 2004. Cave characteristics and speleothems in Xueyu cave group, Fengdu, Chongqing City. Carsologica Sinica 23, 85–90. (in Chinese with English abstract).
Zielinski, G.A., 2000. Use of paleo-records in determining variability within the volcanism-climate system. Quat. Sci. Rev. 19, 417–438.